

Chapter 2

Details of Molecular Bistability Based on Pyrimidine Ring Rotation in Copper(I) Complexes

Abstract The rational molecular design requires a detailed investigation for the equilibrium between two rotational isomers derived from orientation of pyrimidine ring. I studied on chemistry of rotational equilibrium in newly synthesized copper(I) complexes bearing two bidentate ligands, pyridylpyrimidine and bulky diphosphine, using ^1H NMR and single crystal X-ray structural analysis. I found that ion-pairing sensitivities of rotational bistability in the view point of both thermodynamics and kinetics, evidence for intramolecular process of interconversion, and suitability of common organic solution state for the desired function.

Keywords Copper complex • Molecular rotation • Isomerization • Ion pairing • Dynamic NMR

2.1 Introduction

2.1.1 Ion Paring in Metal Complexes

An ion pair consists an equilibrium between several different states that include the anion and cation present as a solvated contact ion pair (CIP), a solvent-shared ion pair, a solvent-separated ion pair (SSIP), and as unpaired solvated ions (Fig. 2.1) [1]. Since ion pairing between the metal complex cation and counter anion [2] (Fig. 2.1.) has often been found to play a key role in functionalization of molecular systems, detailed studies [2–10] on the solvation are valid for the development of promising materials. The ion-pairing behavior of transition metal complexes has been extensively investigated using nuclear magnetic resonance (NMR) techniques such as diffusion-ordered spectroscopy and pulsed gradient spin-echo diffusion studies [2–6]. Ion-paring causes signal splitting in the ^1H NMR spectra of enantiomers of metal complexes bound to a chiral anion [7–10]. In addition, the rate of the chemical exchange between such enantiomers can be determined from the peaks in the spectra at several temperatures [7–10].

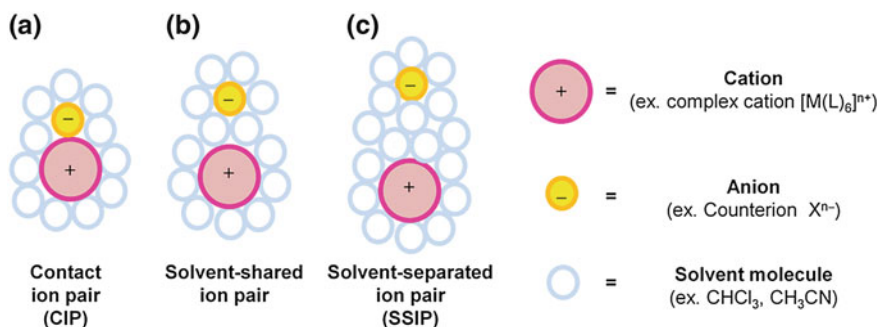


Fig. 2.1 Conceptual diagram showing transition-metal ion pairs. **a** The two contact ion pairs as outer-sphere ion pairs (CIP), **b** solvent-shared, and **c** solvent-separated ion pairs (SSIP)

2.1.2 The Aim of this Study

As I described in Sect. 1.5, pyrimidine ring rotation in copper(I) complexes is a promising system which exhibits the desired functions. The aim of this study is to examine the details of the rotational equilibrium, including ion pairing sensitivities, based on a family of $[Cu(\text{diimine})(\text{diphosphine})]^+$ complexes.

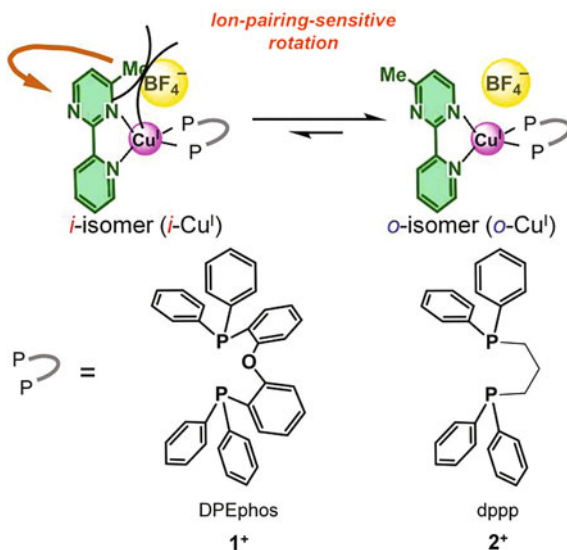
2.1.3 Molecular Design

As described in Sect. 1.2, a family of $[Cu(\text{diimine})(\text{diphosphine})]^+$ complexes has been particularly well studied owing to their intense luminescence; therefore, this class of compounds can be promising candidate for photofunctionalization of our rotational system. I describe here rotational equilibrium in newly synthesized copper(I) complexes bearing a bidentate pyridylpyrimidine and a bulky diphosphine, $1 \cdot BF_4$ ($1^+ = [Cu(\text{Mepypm})(\text{DPEphos})]^+$, Mepypm = 4-methyl-2-(2'-pyridyl)pyrimidine, DPEphos = bis[2-(diphenylphosphino)phenyl]ether), $1 \cdot B(C_6F_5)_4$, $2 \cdot BF_4$ ($2^+ = [Cu(\text{Mepypm})(\text{dppp})]^+$, dppp = 1,3-bis(diphenylphosphino)propane), and $2 \cdot B(C_6F_5)_4$ (Fig. 2.2). I employed $4 \cdot BF_4$ ($4^+ = [Cu(\text{bpy})(\text{DPEphos})]^+$, bpy = 2,2'-bipyridine) as a reference compound. Two kinds of non-coordinative counterions are considered [11–14], BF_4^- and $B(C_6F_5)_4^-$, where the latter is much larger than the former. The chemical equilibrium of the coordination isomers is illustrated in Fig. 2.2, where the notation of the inner ($i\text{-Cu}^I$) and outer ($o\text{-Cu}^I$) isomers describes the orientation of the pyrimidine ring.

2.1.4 Contents of this Chapter

In the present study, I investigated ion pair effects on a metal complex bistability caused by intramolecular ligating atom exchange using newly synthesized

Fig. 2.2 Conceptual diagram showing the effects of ion pairing on the chemical equilibrium of pyrimidine ring rotational isomerization



heteroleptic copper(I) complexes bearing an unsymmetrically substituted pyridylpyrimidine and a bulky diphosphine ligand, **1**·BF₄, **1**·B(C₆F₅)₄, **2**·BF₄, and **2**·B(C₆F₅)₄. I found that the complex exhibited the rotational bistability in common organic solvent, and the ratio of *i*-Cu^I and *o*-Cu^I was solvent- and counterion-sensitive (Fig. 2.2). Two rotational isomers of **2**⁺ were separately obtained as single crystals, and the structure of each isomer was examined in detail from X-ray structural analysis. The values of enthalpy and entropy for rotational equilibrium between *i*-Cu^I and *o*-Cu^I are strongly dependent on the geometry of the diphosphine, polarity of the solvent, and the size of the counterion. Consideration of solvated counter ion pairing is a key point for rationally accounting for the effect of the weak interaction on rotational equilibrium. Since the major part of the copper center bonding surface was occupied by ligands, the position of the counterion affects the orientation of the pyrimidine moiety. I elucidate kinetics of rotational equilibrium between *i*-Cu^I and *o*-Cu^I. The interconversion between the two rotational isomers is generally an intramolecular process, as confirmed by ¹H NMR analysis of a mixed solution of two kinds of complexes.

2.2 Experimental Section

Materials. Tetrakis(acetonitrile)copper(I) tetrafluoroborate ([Cu(MeCN)₄]BF₄) [11], tetrakis(acetonitrile)copper(I) tetrakis(pentafluorophenyl)borate ([Cu(MeCN)₄]B(C₆F₅)₄) [12], and 4-methyl-2-(2'-pyridyl)pyrimidine(Mepypm) [15, 16], were prepared according to literature protocols. Bis[2-(diphenylphosphino)phenyl]ether (DPEphos) was purchased from Wako Pure Chemical

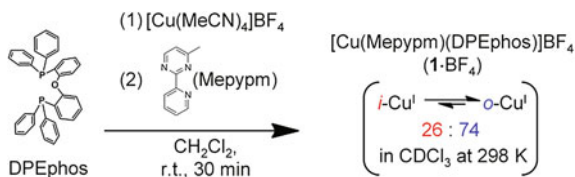
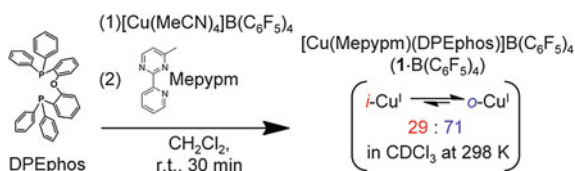
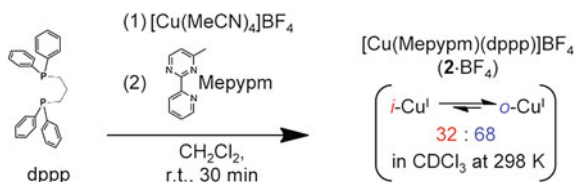
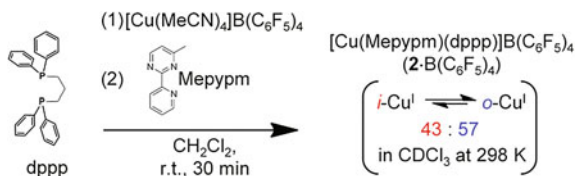
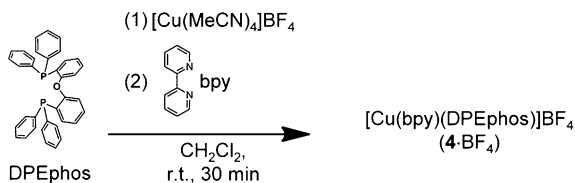
Industries, Ltd. 2,2'-Bipyridine (bpy) and 1,3-bis(diphenylphosphino)propane (dppp) were purchased from Kanto Chemicals. Other chemicals were used as purchased.

Synthesis of [Cu(Mepypm)(DPEphos)]BF₄ (1·BF₄) (Scheme 2.1). A new compound, 1·BF₄, was synthesized according to a modified literature procedure [17, 18]. In this synthesis, [Cu(MeCN)₄]BF₄ (64 mg, 0.20 mmol) was added to DPEphos (121 mg, 0.23 mmol) in 5 mL of dichloromethane. Mepypm (34 mg, 0.20 mmol) in 5 mL of dichloromethane was then added, upon which the reaction solution immediately turned yellow. The reaction mixture was subsequently stirred for an additional 30 min. Diethyl ether was then added to the solution in order to precipitate the product as a yellow solid, which was filtered and washed with diethyl ether. Reprecipitation from a dichloromethane and diethyl ether mixture afforded 1·BF₄ as a yellow solid with a yield of 68 % (116 mg, 0.14 mmol). ¹H NMR (500 MHz, CDCl₃, 253 K) δ 8.86 (d, *J* = 5 Hz, *i*-1H), 8.77 (d, *J* = 8 Hz, *o*-1H), 8.69 (d, *J* = 8 Hz, *i*-1H), 8.65 (d, *J* = 5 Hz, *o*-1H), 8.36 (d, *J* = 5 Hz, *i*-1H), 8.32 (d, *J* = 5 Hz, *o*-1H), 8.04 (t, *J* = 8 Hz, *o*-1H), 8.00 (t, *J* = 8 Hz, *i*-1H), 7.5–6.5 (m), 2.66 (s, *o*-3H), 2.31 (s, *i*-3H). Elemental analysis. Calculated for C₄₆H₃₇N₃OP₂CuBF₄: C 64.24, H 4.34, N 4.89, found C 64.19, H 4.48, N 4.78.

Synthesis of [Cu(Mepypm)(DPEphos)]B(C₆F₅)₄ (1·B(C₆F₅)₄) (Scheme 2.2). A new compound, 1·B(C₆F₅)₄, was synthesized using a procedure similar to that described for 1·BF₄ with the exception that hexane was used in place of diethyl ether. [Cu(MeCN)₄]B(C₆F₅)₄ (80 mg, 0.088 mmol), DPEphos (59 mg, 0.11 mmol), and Mepypm (14 mg, 0.082 mmol): Yellow solid (70 %, 83 mg). ¹H NMR (500 MHz, CDCl₃, 253 K) δ 8.76 (m, *o*-1H + *i*-1H), 8.68 (d, *J* = 7.7 Hz, *i*-1H), 8.37 (d, *J* = 5.5 Hz, *o*-1H), 8.29 (d, *J* = 5.5 Hz, *o*-1H), 8.26 (d, *J* = 4.8 Hz, *i*-1H), 7.99 (t, *J* = 7.8 Hz, *o*-1H), 7.95 (t, *J* = 7.6 Hz, *i*-1H), 7.4–6.7 (m, *i*-30H + *o*-30H), 2.63 (s, *o*-3H), 2.29 (s, *i*-3H). Elemental analysis. Calculated for C₇₀H₃₇N₃OP₂CuBF₂₀: C 57.89, H 2.57, N 2.89, found C 58.16, H 2.87, N 2.77.

Synthesis of [Cu(Mepypm)(dppp)]BF₄ (2·BF₄) (Scheme 2.3). A new compound, 2·BF₄, was synthesized using a procedure similar to that described for 1·BF₄. [Cu(MeCN)₄]BF₄ (67 mg, 0.20 mmol), dppp (104 mg, 0.25 mmol), and Mepypm (34 mg, 0.20 mmol): Yellow solid (56 %, 82 mg). ¹H NMR (500 MHz, CDCl₃, 253 K) δ 8.97 (d, *J* = 5.0 Hz *i*-1H), 8.93 (d, *J* = 7.9 Hz, *i*-1H), 8.85 (d, *J* = 7.9 Hz, *o*-1H), 8.79 (d, *J* = 5.5 Hz, *o*-1H), 8.47 (d, *J* = 5.1 Hz, *o*-1H), 8.35 (d, *J* = 5.2 Hz, *i*-1H), 8.20 (t, *J* = 7.8 Hz, *i*-1H), 8.11 (t, *J* = 7.7 Hz, *o*-1H), 7.69 (dd, *J* = 7.5, 5.1 Hz, *i*-1H), 7.62 (dd, *J* = 7.5, 5.2 Hz, *o*-1H), 7.5–7.1 (m, *i*-29H + *o*-29H), 2.88 (m, br), 2.69 (s + br), 2.45 (t, br), 2.32 (s, *i*-3H), 2.10 (m, br). Elemental analysis. Calculated for C₃₇H₃₅N₃P₂CuBF₄: C 60.54, H 4.81, N 5.73, found C 60.52, H 4.92, N 5.49.

Synthesis of [Cu(Mepypm)(dppp)]B(C₆F₅)₄ (2·B(C₆F₅)₄) (Scheme 2.4). A new compound, 2·B(C₆F₅)₄, was synthesized using a procedure similar to that described for 1·B(C₆F₅)₄ by employing [Cu(MeCN)₄]B(C₆F₅)₄ (185 mg, 0.20 mmol), dppp (92 mg, 0.22 mmol), and Mepypm (35 mg, 0.21 mmol). Yellow solid (40 %, 108 mg). ¹H NMR (500 MHz, CDCl₃, 253 K) δ 8.91 (d, *J* = 8.0 Hz, *i*-1H), 8.88 (m, *i*-1H + *o*-1H), 8.29 (d, *J* = 5.1 Hz, *o*-1H), 8.26 (d, *J* = 4.7 Hz,

Scheme 2.1 Synthesis of 1·BF₄**Scheme 2.2** Synthesis of 1·B(C₆F₅)₄**Scheme 2.3** Synthesis of 2·BF₄**Scheme 2.4** Synthesis of 2·B(C₆F₅)₄**Scheme 2.5** Synthesis of 4·BF₄

i-1H), 8.18 (d, *J* = 5.5 Hz, *o*-1H), 8.14 (t, *J* = 7.8 Hz, *i*-1H), 8.09 (t, *J* = 7.9 Hz, *o*-1H), 7.59 (dd, *J* = 7.4, 5.3 Hz, *i*-1H), 7.50 (dd, *J* = 7.3, 5.4 Hz, *o*-1H), 7.4–7.1 (m, *i*-30H + *o*-30H), 2.87 (m, br), 2.69 (s + *o*-3H), 2.57 (m, br), 2.35 (m, br), 2.23 (s, *i*-3H), 2.14 (m, br). Elemental analysis. Calculated for C₆₁H₃₅N₃P₂CuBF₂₀: C 55.24, H 2.66, N 3.17, found C 55.10, H 2.86, N 3.13.

Synthesis of [Cu(bpy)(DPEphos)]BF₄ (4·BF₄) (Scheme 2.5). [Cu(bpy)(DPEphos)]BF₄ was prepared according to literature methods [19]. [Cu(bpy)(DPEphos)]BF₄ was synthesized using a procedure similar to that described for 1·B(C₆F₅)₄ by employing [Cu(MeCN)₄]BF₄ (32 mg, 0.10 mmol), DPEphos

(59 mg, 0.11 mmol), and bpy (16 mg, 0.10 mmol). Yellow solid (78 %, 66 mg, 0.078 mmol). ^1H NMR (500 MHz, CDCl_3 293 K) δ 8.49 (d, $J = 7.6$ Hz, py_3), 8.33 (d, $J = 5.2$ Hz, py_6), 8.04 (t, $J = 8.0$ Hz, py_4), 7.3–6.7 (m, Ph and py_5). Elemental analysis. Calculated for $\text{C}_{46}\text{H}_{36}\text{N}_2\text{OP}_2\text{CuBF}_4$: C 65.38, H 4.29, N 3.31, found C 65.17, H 4.50, N 3.27.

X-ray Structural Analysis. Yellow single crystals of $o\text{-1}\cdot\text{BF}_4\cdot\text{CHCl}_3$, $o\text{-1}\cdot\text{B}(\text{C}_6\text{F}_5)_4\cdot 1.5\text{hexane}$, $o\text{-2}\cdot\text{BF}_4\cdot 0.5\text{MeOH}$, and $i\text{-2}\cdot\text{B}(\text{C}_6\text{F}_5)_4$ were obtained by slow diffusion of diethyl ether into a chloroform solution of $\mathbf{1}\cdot\text{BF}_4$, slow diffusion of hexane into a dichloromethane solution of $\mathbf{1}\cdot\text{B}(\text{C}_6\text{F}_5)_4$, diethyl ether into a methanol solution of $\mathbf{2}\cdot\text{BF}_4$, and hexane into a chloroform solution of $\mathbf{2}\cdot\text{B}(\text{C}_6\text{F}_5)_4$, respectively. Diffraction data were collected on an AFC10 diffractometer with monochromated MoK_α radiation ($\lambda = 0.7107$ Å). Lorentz polarization and numerical absorption corrections were performed with the Crystal Clear 1.3.6 program. The structure was solved by the direct method using SIR 92 software [20] and refined against F^2 using SHELXL-97 [21]. WinGX software was used to prepare the material for publication [22]. Crystallographic data are listed in Table 2.1. Disordered counterions in $o\text{-2}\cdot\text{BF}_4$ were analyzed by PART, SIMU, and SADI options. The disordered methanol molecule in $o\text{-2}\cdot\text{BF}_4$ was analyzed by PART, EADP, and SADI options.

Instruments. NMR spectra at several temperatures in the dark were recorded on a Bruker DRX 500 spectrometer, using a ca. 20 min data-recording interval. The experimental ^1H NMR spectra were simulated using iNMR 2.6.5 software. The reported chemical shifts of the solvent peaks were used for calibration of the NMR spectra in CDCl_3 (tetramethylsilane $\delta = 0$ ppm), CD_2Cl_2 ($\delta = 5.32$ ppm), acetone- d_6 ($\delta = 2.05$ ppm) and acetonitrile- d_3 (CD_3CN , $\delta = 1.94$ ppm) [23].

Thermodynamic and Kinetic Analysis. The analysis was performed using the aromatic ^1H NMR signals of the Mepypm moiety. The results of $\mathbf{1}\cdot\text{BF}_4$ in CDCl_3 , acetone- d_6 , and CD_3CN were comparable with values, which were based on the methyl group of the Mepypm moiety. The solution state molar ratios of the isomers at several temperatures were determined from ^1H NMR signal integration. The broad spectra acquired at room temperature were excluded from the thermodynamic analysis. The generated van't Hoff plots [24] were based on an equilibrium constant corresponding to the value of $[\text{o-Cu}^{\text{I}}]/[\text{i-Cu}^{\text{I}}]$. The molar ratios of the $o\text{-Cu}^{\text{I}}$, x_o , which is equal to $100 \times [\text{o-Cu}^{\text{I}}]/([\text{i-Cu}^{\text{I}}] + [\text{o-Cu}^{\text{I}}])$ %, at variable temperatures were calculated by extrapolating the van't Hoff plots. The values of x_{o298} were estimated from predicted value of “ $\ln K$ ” at “ $1/T$ ” = $1/298$ K^{-1} using single linear regression of van't Hoff plots. Root-mean-square error, s , which reflects the error of the predicted value ($\ln K$), is less than 0.017 in all data as we tested. The value, 0.017, corresponds to the 0.5 % in x_{o298} . Since the value of x_{o298} is an extrapolation number, we performed t test to consider the error of x_{o298} . The value is within $x_{o298} - 1 \% < x_{o298} < x_{o298} + 1 \%$ in 95 % significance level, even if in the case of the largest error data. The thermodynamic parameters for the $i\text{-Cu}^{\text{I}} \rightarrow o\text{-Cu}^{\text{I}}$ rotation (ΔH , ΔS , ΔG), K , and x_o can be represented by the following van't Hoff equations:

Table 2.1 Crystallographic data of *o*-1·BF₄·CHCl₃, *o*-1·B(C₆F₅)₄·1.5hexane, *o*-2·BF₄·0.5MeOH, and *i*-2·B(C₆F₅)₄

	<i>o</i> -1·BF ₄ · CHCl ₃	<i>o</i> -1·B(C ₆ F ₅) ₄ · 1.5hexane	<i>o</i> -2·BF ₄ · 0.5MeOH	<i>i</i> -2·B(C ₆ F ₅) ₄
Molecular formula	C ₄₇ H ₃₈ BCl ₃ Cu F ₄ N ₃ OP ₂	C ₇₉ H ₅₈ BCu F ₂₀ N ₃ OP ₂	C _{37.5} H _{36.5} BCu F ₄ N ₃ O _{0.5} P ₂	C ₆₁ H ₃₅ BCu F ₂₀ N ₃ P ₂
Mw/g mol ⁻¹	979.44	1581.57	749.49	1326.21
Crystal system	Triclinic	Triclinic	Triclinic	Monoclinic
Space group	P – 1	P – 1	P – 1	P21/c
<i>T</i> /K	113	113(2)	93(2)	113(2)
<i>a</i> /Å	9.661(4)	12.822(3)	12.179(5)	9.2522(12)
<i>b</i> /Å	13.796(5)	15.851(4)	15.881(6)	35.880(5)
<i>c</i> /Å	19.080(7)	19.419(5)	19.374(7)	16.941(2)
α /°	96.296(5)	78.530(10)	99.093(5)	90
β /°	94.822(3)	84.282(12)	95.012(2)	105.400(2)
γ /°	107.981(6)	67.436(9)	107.070(7)	90
<i>V</i> /Å ³	2385.5(16)	3570.5(15)	3502(2)	5422.1(13)
<i>Z</i>	2	2	4	4
Reflections collected	18299	28309	28206	42927
Independent reflections	10336	15651	15429	12256
<i>R</i> _{int}	0.0194	0.0541	0.0619	0.0431
ρ_{calcd} /g cm ⁻³	1.36	1.471	1.62	1.62
λ /Å	0.7107	0.7107	0.7107	0.7107
μ /cm ⁻¹	0.746	0.452	0.77	0.577
<i>R</i> ₁ ^a	0.094	0.0900	0.0988	0.0642
<i>wR</i> ₂ ^b	0.2827	0.2046	0.2381	0.1416
GOF ^c	1.039	1.101	1.174	1.174

^a $R_1 = \sum ||F^o| - |F^c|| / \sum |F^o|$ ($I > 2\sigma(I)$)^b $wR_2 = [\sum (w(F^{o2} - F^{c2})^2) / \sum w(F^{o2})^2]^{1/2}$ ($I > 2\sigma(I)$)^c $\text{GOF} = [\sum (w(F^{o2} - F^{c2})^2) / \sum (N^r - N^p)]^{1/2}$

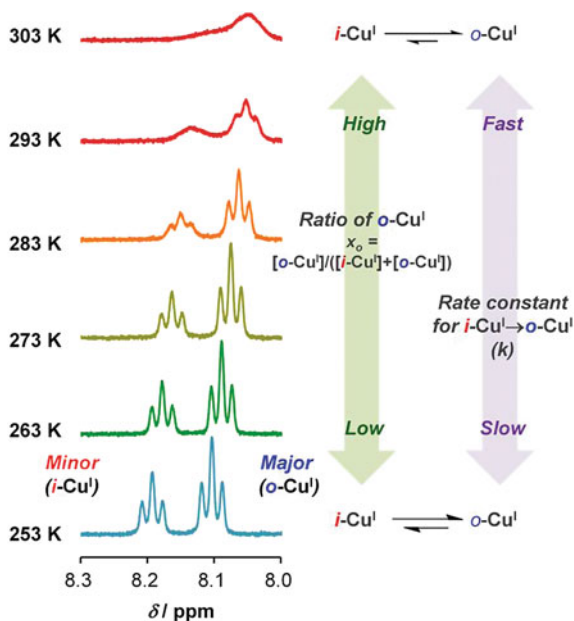
$$\ln \{x_o / (100 - x_o)\} = \ln K = -\Delta G / RT = -\Delta H / RT + \Delta S / R \quad (2.1)$$

Here, *T* corresponds to the absolute temperature and *R* is gas constant (8.314 J K⁻¹ mol⁻¹). The rate constants for the *i*-Cu^I → *o*-Cu^I isomerization, *k*, at several temperatures were determined from simulation analysis of the NMR spectra using the equilibrium constants determined from the van't Hoff plots. *k* at variable temperatures was calculated from the extrapolations of the Arrhenius plots [24]:

$$\ln k = -E_a / RT + \ln (A) \quad (2.2)$$

Here, *E*_a and *A* correspond to the activation energy and frequency factor of the *i* → *o*-isomerization, respectively.

Fig. 2.3 Aromatic ^1H NMR signals of a Mepypm moiety in 2-BF_4 in CDCl_3 at several temperatures. The signals derived from $i\text{-Cu}^{\text{I}}$ and $o\text{-Cu}^{\text{I}}$ are represented as red and blue, respectively. Illustration of the ratios and the rate of the rotational equilibrium is also described on the right side



2.3 Synthesis and Characterization of Rotational Equilibrium in Solution

New compounds, 1-BF_4 , $1\text{-B}(\text{C}_6\text{F}_5)_4$, 2-BF_4 , and $2\text{-B}(\text{C}_6\text{F}_5)_4$, were synthesized using a modified literature method (Sect. 2.2) [17–19]. In this approach, tetrakis(acetonitrile)copper(I) salt was reacted with a diphosphine ligand and a Mepypm ligand in dichloromethane at room temperature. The obtained compounds were characterized by ^1H NMR and elemental analysis.

The rotational bistability of 1-BF_4 in CDCl_3 , CD_2Cl_2 , acetone- d_6 , CD_3CN and $1\text{-B}(\text{C}_6\text{F}_5)_4$ in CDCl_3 , 2-BF_4 in CDCl_3 , dichloromethane- d_2 (CD_2Cl_2), acetone- d_6 , acetonitrile- d_3 (CD_3CN), and $2\text{-B}(\text{C}_6\text{F}_5)_4$ in CDCl_3 was characterized using ^1H NMR analysis to monitor chemical exchange (Figs. 2.3, 2.4, 2.5, 2.6, 2.7, 2.8, 2.9, 2.10, 2.11, 2.12, 2.13). Integration of ^1H NMR spectra along with line-shape analysis are well-established methods [25, 26] for investigating the thermodynamics and kinetics of a chemical equilibrium [25–36].

For example, two clearly resolved sets of signals were observed in the ^1H NMR spectrum of 2-BF_4 in CDCl_3 at 253 K. A major singlet peak at $\delta = 2.69$ ppm and a minor one at $\delta = 2.32$ ppm were assigned as a methyl group of $o\text{-Cu}^{\text{I}}$ and $i\text{-Cu}^{\text{I}}$, respectively, because of considerations as follows. (i) The chemical shift of the methyl group of $o\text{-Cu}^{\text{I}}$ is expected to resemble that of Mepypm ($\delta = 2.67$ ppm, CDCl_3 at 293 K), owing to an absence of shielding effects caused by a copper center and phenyl groups on a diphosphine moiety. (ii) The shielding effects on $i\text{-Cu}^{\text{I}}$ methyl group, which is close to both the copper and the diphosphine moieties,

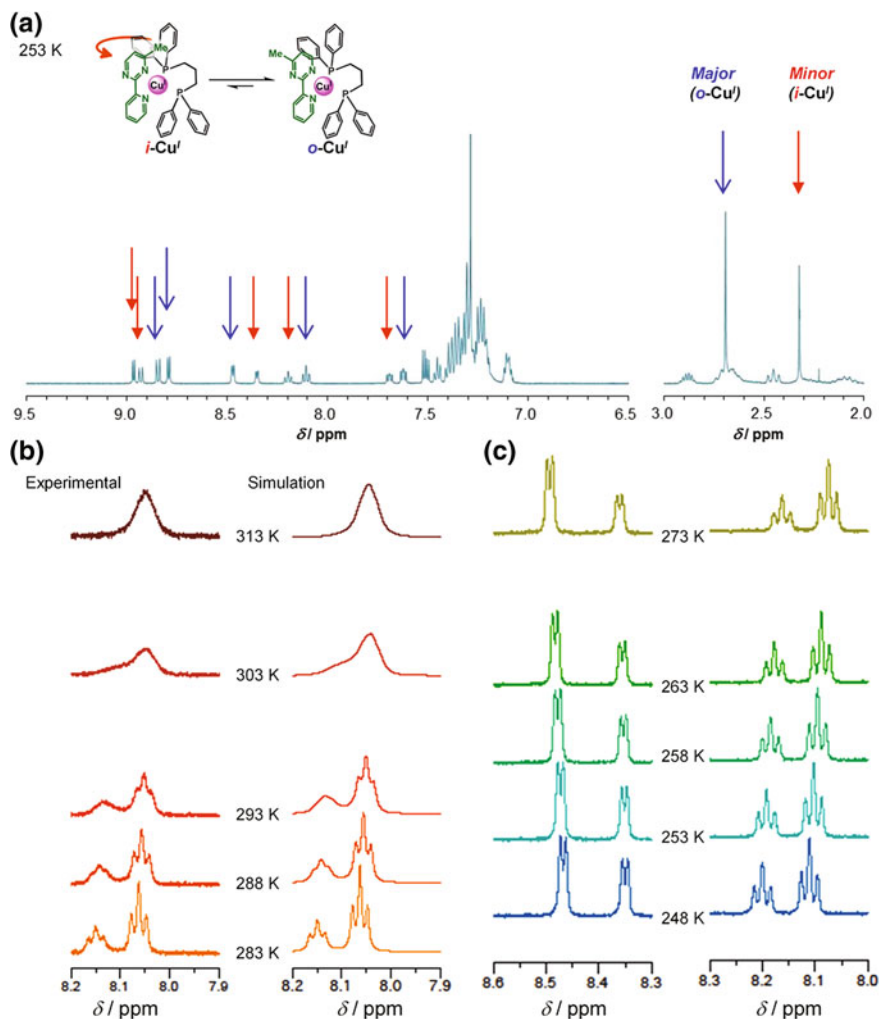


Fig. 2.4 **a** Experimental ^1H NMR spectra of $2\cdot\text{BF}_4$ in CDCl_3 at 253 K. The signals derived from *i*-Cu^I and *o*-Cu^I are represented as red and blue, respectively. **b** Experimental (left) and simulated (right) ^1H NMR spectra at 313, 303, 293, and 283 K. **c** Experimental ^1H NMR spectra at 273, 263, 258, 253, and 248 K

are expected to cause an upfield shift of the signal. Signal splitting was also observed in the aromatic proton signals of the Mepypm ligand (Fig. 2.3). The ratio of *o*-Cu^I, estimated from integration of the minor and major signals, is represented as $x_o\%$. The ratio of *i*-isomer is thus $(100 - x_o)\%$. Consider for instance that at 253 K, the x_o value was determined to be 60 %; the reason of higher x_o values at higher temperature is described in later sections. Upon heating, these signals broadened, indicating that two isomers, *i*-Cu^I and *o*-Cu^I, interconverted in solution

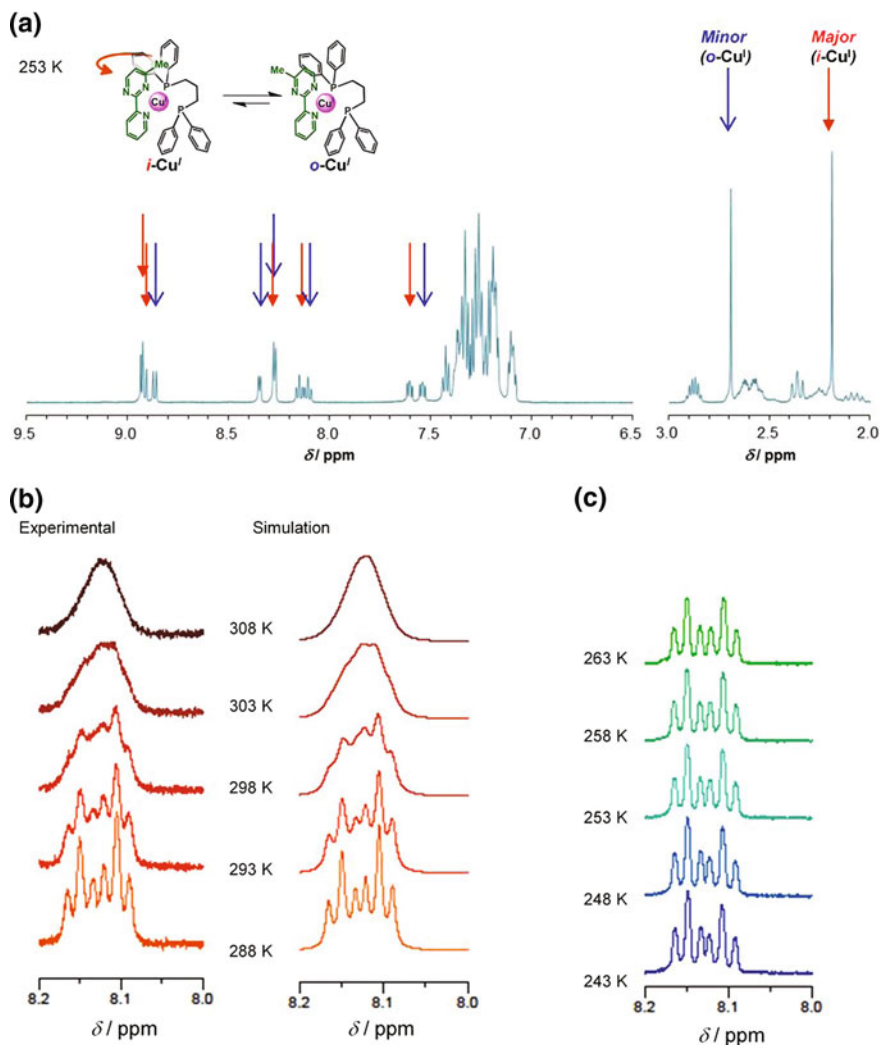


Fig. 2.5 **a** Experimental ¹H NMR spectra of 2-BF₄ in CD₂Cl₂ at 253 K. **b** Experimental (left) and simulated (right) ¹H NMR spectra at 308, 303, 298, 293, and 288 K. **c** Experimental ¹H NMR spectra at 263, 258, 253, 248, and 243 K

on a timescale that is commensurate with that of the ¹H NMR measurement (Fig. 2.3). The rate constant for the *i*-Cu^I → *o*-Cu^I isomerization, *k*, was estimated from simulated fittings of the broadened ¹H NMR spectra (Fig. 2.3). For example, the value of *k* was 100 s⁻¹ at 303 K; faster rate of the rotation at higher temperature is normal for chemical equilibrium. These parameters, at several temperatures and under various conditions, were determined by the same analysis as that described above.

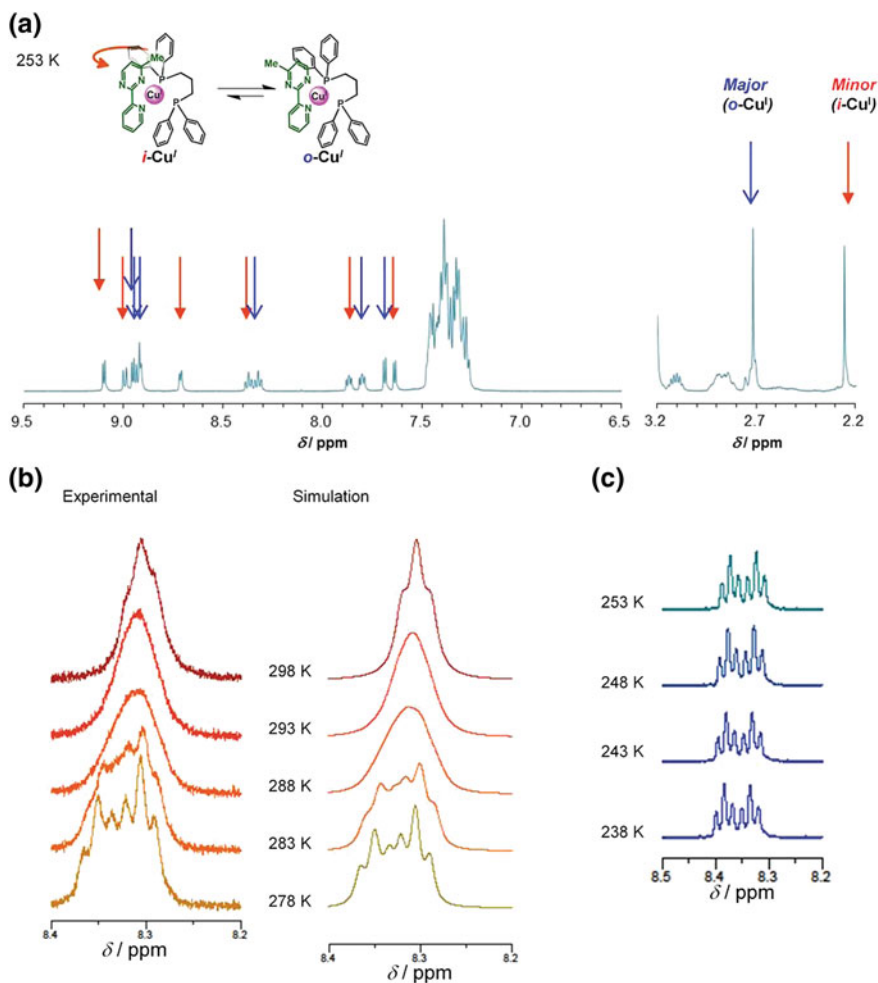


Fig. 2.6 **a** Experimental ¹H NMR spectra of **2**·BF₄ in acetone-*d*₆ at 253 K. **b** Experimental (*left*) and simulated (*right*) ¹H NMR spectra at 298, 293, 288, 283, and 278 K. **c** Experimental ¹H NMR spectra at 253, 248, 243, and 238 K

¹H NMR spectra of [Cu(bpy)(DPEphos)]BF₄ (**4**·BF₄), which does not undergo rotation, show only one set of signals, supporting that the signal separation mentioned above is derived from rotational isomers.

The *i*-Cu^I to *o*-Cu^I ratios and their heat-sensitivities, along with isomerization rates, are dependent on the solvent and counterion (Figs. 2.4, 2.5, 2.6, 2.7, 2.8, 2.9, 2.10, 2.11, 2.12, 2.13). However, a complete description of the observed effects requires a close consideration of the geometry of the complexes, as highlighted in later sections.

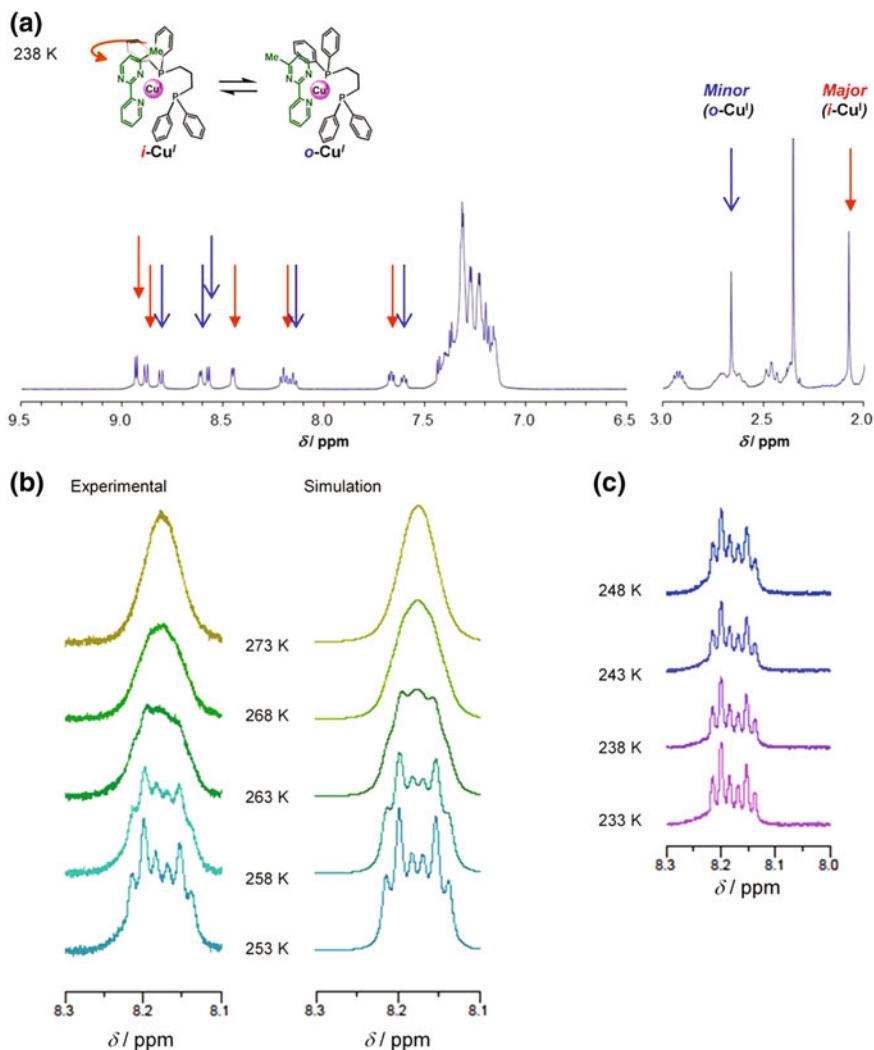


Fig. 2.7 **a** Experimental ¹H NMR spectra of **2**·BF₄ in CD₃CN at 238 K. **b** Experimental (*left*) and simulated (*right*) ¹H NMR spectra at 273, 268, 263, 258, and 253 K **c** Experimental ¹H NMR spectra at 248, 243, 238, and 233 K

2.4 Characterization for Intramolecular Process

The interconversion between two isomers, *i*-Cu^I and *o*-Cu^I, is generally an intramolecular ligating atom exchange process, as confirmed by ¹H NMR analysis of a mixed solution of [Cu(Mepypm)(DPEphos)]BF₄ (**1**·BF₄) and [Cu(bpy)(DPEphos)]BF₄ (**4**·BF₄), which does not undergo rotation [19]; This strategy is based on

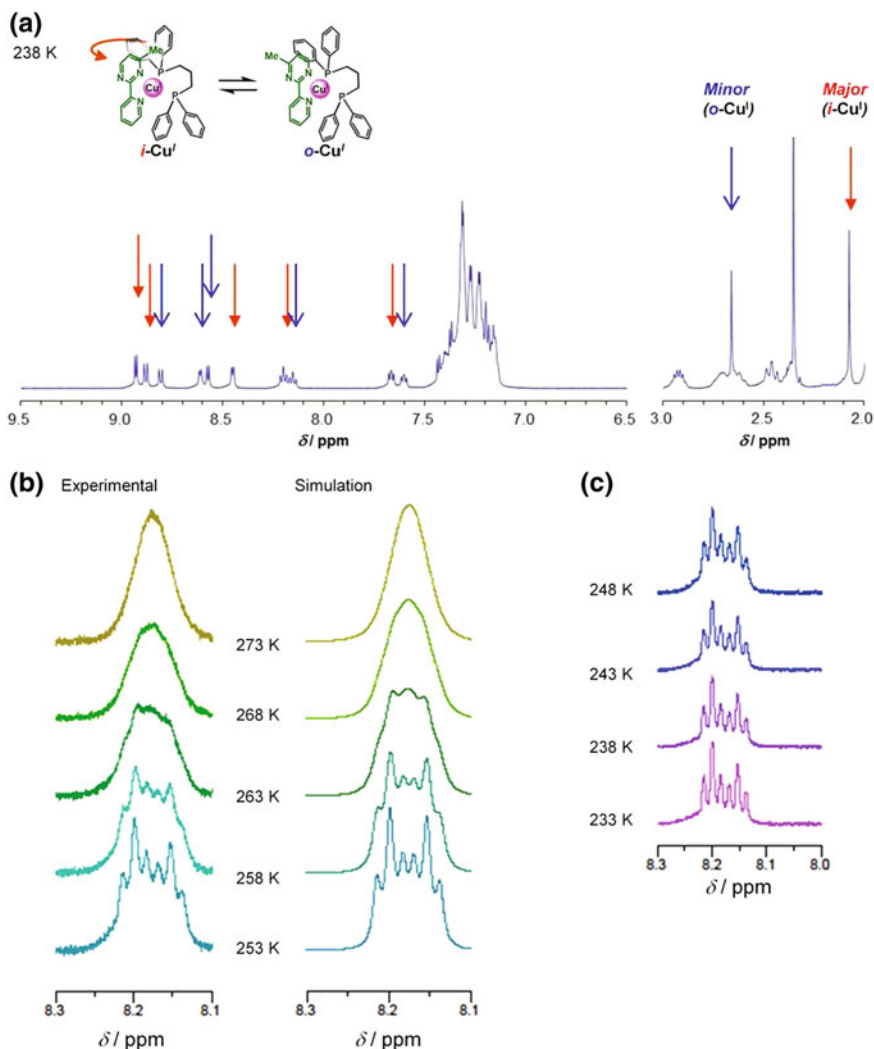


Fig. 2.8 **a** Experimental ¹H NMR spectra of 2·B(C₆F₅)₄ in CDCl₃ at 273 K. **b** Experimental (left) and simulated (right) ¹H NMR spectra at 313, 308, 303, 298, 293, and 288 K. **c** Experimental ¹H NMR spectra at 278, 273, 268, 263, 258, and 253 K

modified method described in literature reported by Shionoya et al. [28]. The rate of interconversion between *i*-Cu^I and *o*-Cu^I (k) via intramolecular process is denoted as k_{intra} , that via intermolecular process is as k_{inter} ($k = k_{\text{intra}} + k_{\text{inter}}$). The value of k_{inter} is evaluated from the rate of interconversion between 4·BF₄ and 1·BF₄, because both processes require intermolecular diimine ligand exchange.

A ¹H NMR spectrum of 4·BF₄ in acetone-*d*₆ at room temperature displayed one set of signals (Fig. 2.14b). Two sets of broadened signals derived from *i*-Cu^I and

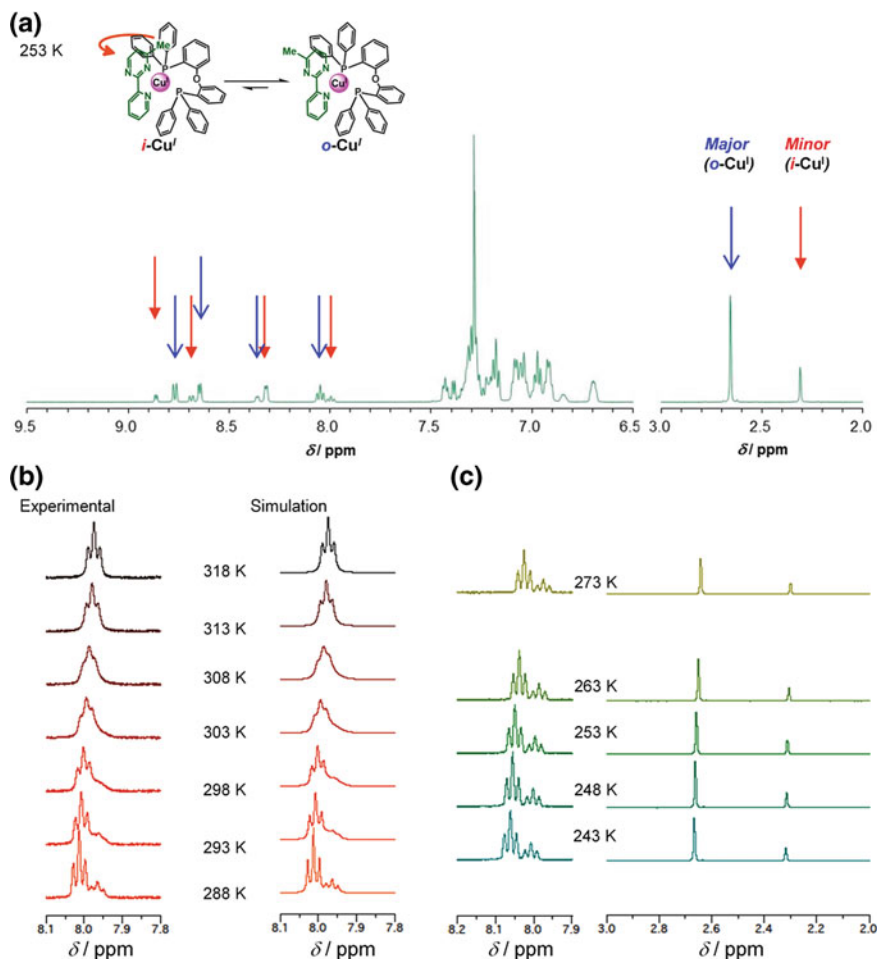


Fig. 2.9 **a** Experimental ^1H NMR spectra of $\mathbf{1}\cdot\text{BF}_4$ in CDCl_3 at 253 K. **b** Experimental (left) and simulated (right) ^1H NMR spectra at 318, 313, 308, 303, 298, 293, and 288 K. **c** Experimental ^1H NMR spectra at 273, 263, 253, 248, and 243 K

o-Cu^I were observed in a ^1H NMR spectrum of $\mathbf{1}\cdot\text{BF}_4$ under the same conditions (Fig. 2.14a). A ^1H NMR spectrum of a mixed solution of $\mathbf{4}\cdot\text{BF}_4$ and $\mathbf{1}\cdot\text{BF}_4$ under the same conditions was simply a superposition of the two spectra (Fig. 2.14c), including signals derived from diphosphine moieties, suggesting that the intermolecular interconversion between $\mathbf{4}\cdot\text{BF}_4$ and $\mathbf{1}\cdot\text{BF}_4$ via diimine ligand exchange reaction was extremely slow compared with the timescale of the ^1H NMR measurement (Fig. 2.14d). In addition, the ^1H NMR of the solution showed no signal broadening derived from $\mathbf{4}\cdot\text{BF}_4$ at 313 K (Fig. 2.15), where the estimated value of k was 300 s^{-1} . The rate constant for the intermolecular process under the given condition (k_{inter}) was smaller than $\text{ca. } 10^0\text{ s}^{-1}$ ($k \gg k_{\text{inter}}$), because signal fusion

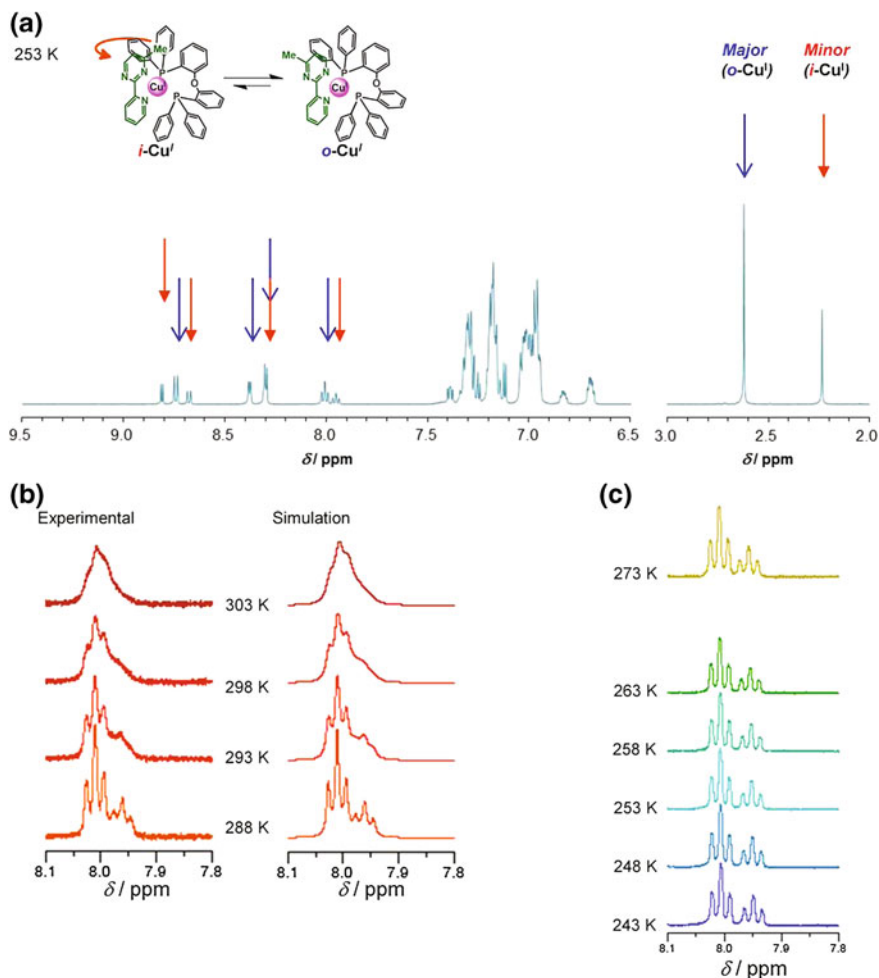


Fig. 2.10 **a** Experimental ¹H NMR spectra of **1**·BF₄ in CD₂Cl₂ at 253 K. **b** Experimental (left) and simulated (right) ¹H NMR spectra at 303, 298, 293, and 288 K. **c** Experimental ¹H NMR spectra at 273, 263, 258, 253, 248, and 243 K

derived from two species is observed when rate of chemical exchange between them is over a time scale of ¹H NMR (ca. 10⁰ s⁻¹). Therefore, interconversion between *i*-Cu^I and *o*-Cu^I in typical organic solvents at ambient temperature is dominated by intramolecular process ($k_{\text{intra}} \gg k_{\text{inter}}$). Possibilities of faster intermolecular process ($k_{\text{intra}} \sim k_{\text{inter}}$ or $k_{\text{intra}} \ll k_{\text{inter}}$) can be denied from small difference in signal broadness between three species derived from *i*-, *o*-isomers of **1**·BF₄ and **4**·BF₄. This interpretation is supported by the fact that the shape of the peaks in the ¹H NMR spectra of **1**·BF₄ in acetone-*d*₆ at room temperature displayed no dependence on concentration (Fig. 2.16).

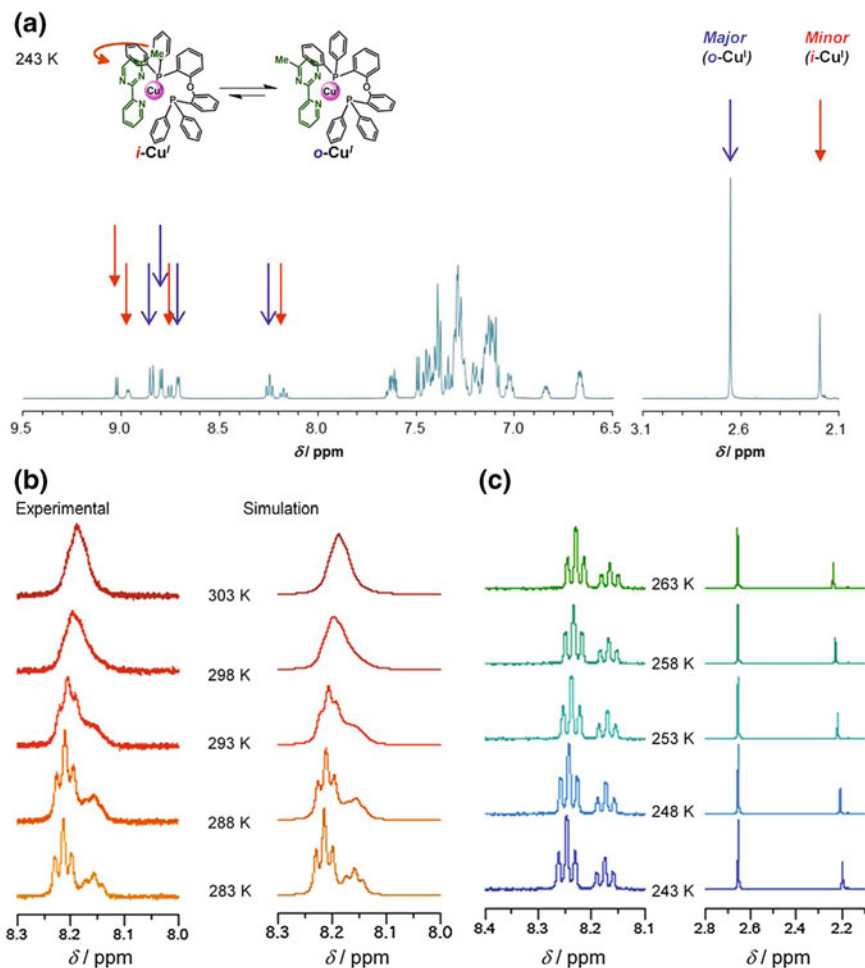


Fig. 2.11 **a** Experimental ¹H NMR spectra of **1**·BF₄ in acetone-*d*₆ at 243 K. **b** Experimental (*left*) and simulated (*right*) ¹H NMR spectra at 303, 298, 293, 288, and 283 K. **c** Experimental ¹H NMR spectra at 263, 258, 253, 248, and 243 K

This conclusion, intramolecular nature of interconversion between two rotational isomers, is additionally evidenced from similar experiment using a mixed solution of [Cu(Mepypm)(dppp)]BF₄ (**2**·BF₄) and [Cu(Mepypm)(DPEphos)]BF₄ (**1**·BF₄), which are different in diphosphine units. A ¹H NMR spectrum of a mixed solution of **2**·BF₄ and **1**·BF₄ (Fig. 2.17c) under the same conditions was simply a superposition of the two spectra of **2**·BF₄ and **1**·BF₄ (Fig. 2.17a, b), including signals derived from Mepypm moieties.

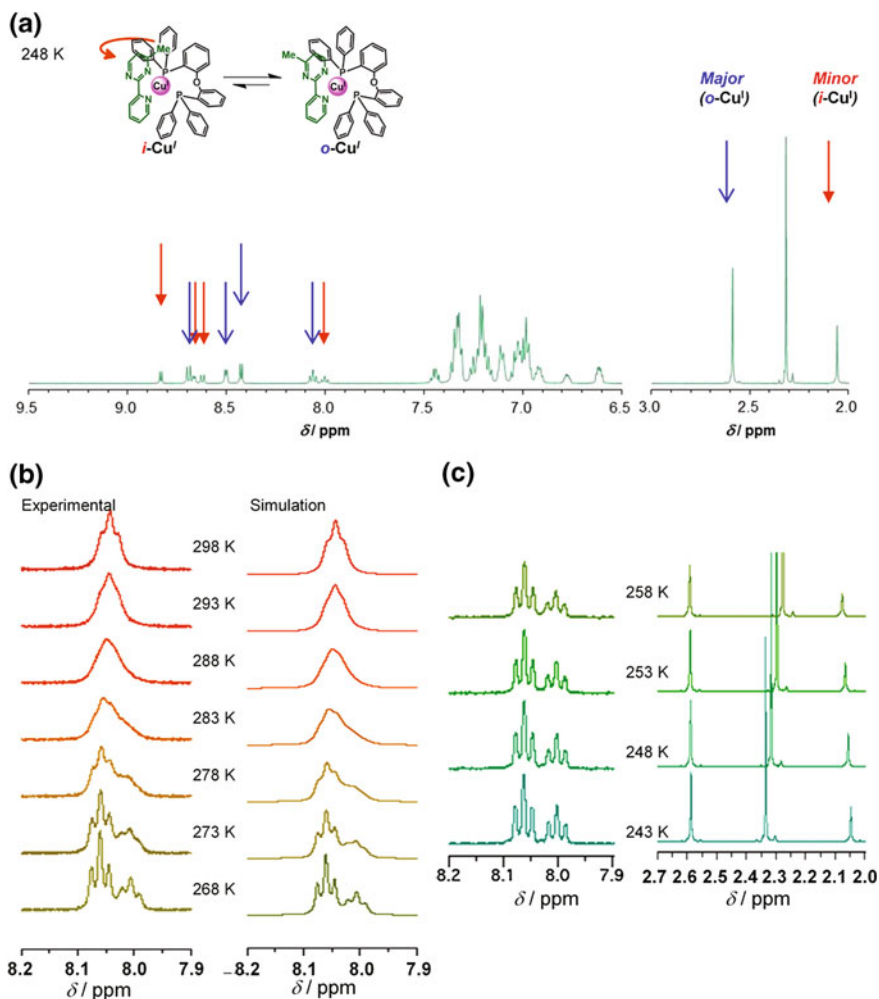


Fig. 2.12 **a** Experimental ¹H NMR spectra of **1**·BF₄ in CD₃CN at 248 K. **b** Experimental (*left*) and simulated (*right*) ¹H NMR spectra at 298, 293, 288, 283, 278, 273, and 268 K. **c** Experimental ¹H NMR spectra at 258, 253, 248, and 243 K

2.5 Crystallography

I performed single crystal X-ray structural analysis of **1**·BF₄, **1**·B(C₆F₅)₄, **2**·BF₄, and **2**·B(C₆F₅)₄ (Figs. 2.18, 2.19, 2.20, 2.21, 2.22, 2.23 and Table 2.1). The ratio of the complex cation to the counterion in the asymmetric unit was 1:1, suggesting that the oxidation state of the metal atom was copper(I) in the single crystal. The geometric parameters of the complex cations in **1**·BF₄, **1**·B(C₆F₅)₄, **2**·BF₄, and **2**·B(C₆F₅)₄ bond lengths were in agreement to the ones of the family of

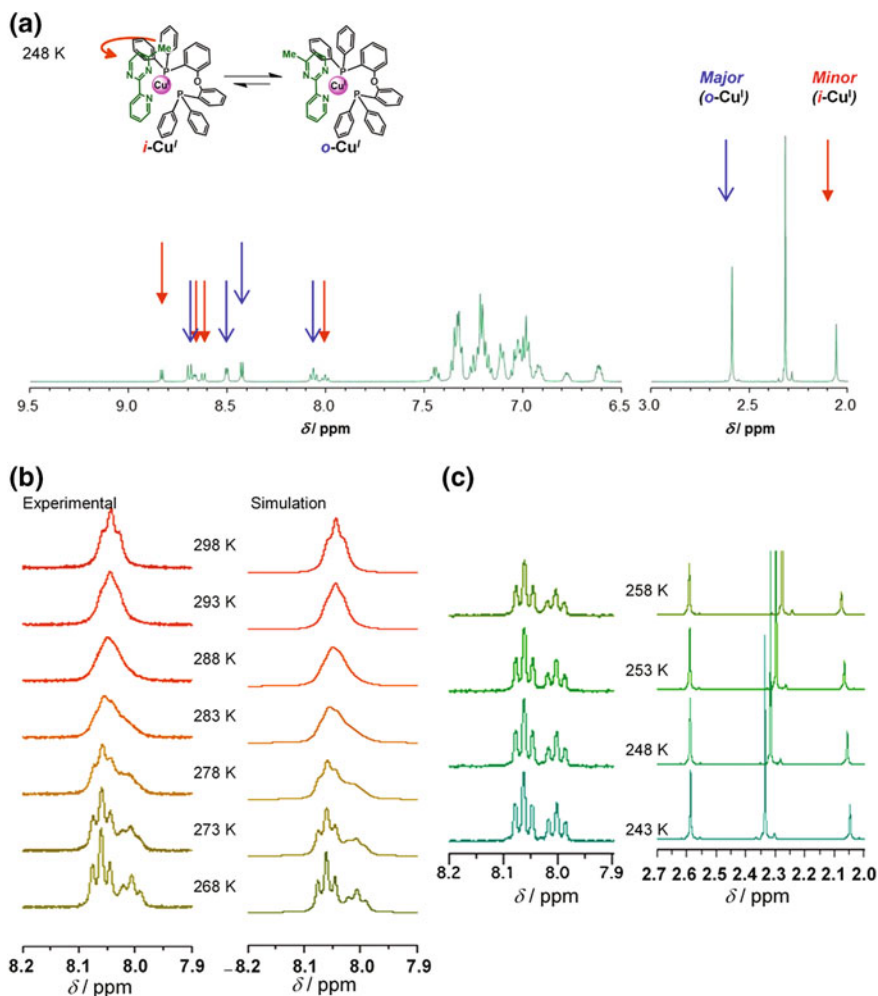


Fig. 2.13 **a** Experimental ^1H NMR spectra of $1\cdot\text{B}(\text{C}_6\text{F}_5)_4$ in CDCl_3 at 248 K. **b** Experimental (*left*) and simulated (*right*) ^1H NMR spectra at 308, 303, 298, 293, and 283 K. **c** Experimental ^1H NMR spectra at 263, 253, 248, and 243 K

$[\text{Cu}(\text{diimine})(\text{diphosphine})]^+$ (Table 2.2) [17, 18]. I note that the distance between oxygen and copper atoms in $1\cdot\text{BF}_4$ is found to be non-bonding region (3.18 Å), which is consistent with well-established geometries in copper(I) complexes bearing two phosphine ligating atoms in the DPEphos unit and two nitrogen ligating atoms in diimine unit; for details, see Sect. 1.2. The methyl group of the Mepypm moiety in $2\cdot\text{BF}_4$ is oriented outward of the metal center, and no disorder was found in the coordination mode. This result suggests that all 2^+ species in the single crystal exist solely as the *o*-isomer, which corresponds to a pyrimidine

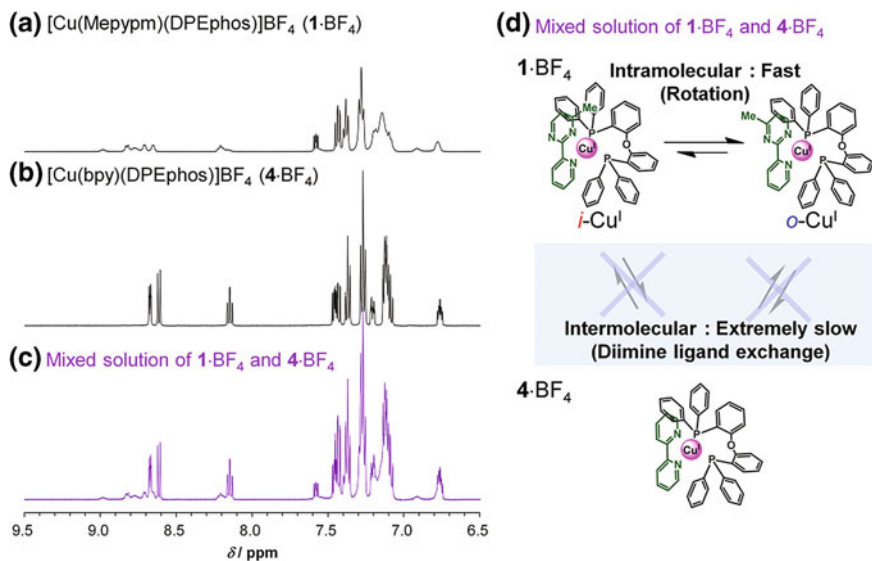


Fig. 2.14 a–c Partial ^1H NMR spectra of 1-BF_4 (a), 4-BF_4 (b), and a mixture of 1-BF_4 and 4-BF_4 (c) in acetone- d_6 in the dark at room temperature. **d** Illustration of the interconversion between species in a mixed solution of 1-BF_4 and 4-BF_4

moiety orientation that is identical to a crystal structure of 1-BF_4 (Figs. 2.18a, c). In contrast, the methyl group in $2\text{-B}(\text{C}_6\text{F}_5)_4$ is directed toward the metal center, indicating that all 2^+ species exist as the i -isomer in the single crystal (Fig. 2.18b). Furthermore, all 1^+ species in $1\text{-B}(\text{C}_6\text{F}_5)_4$ exist as the o -isomer (Fig. 2.18d), which is identical to 1-BF_4 from the viewpoint of pyrimidine orientation. Based on the orientation of pyrimidine in the crystal as well as considering the solvents to have negligible interaction with the complex cation, the four single crystals are denoted as $o\text{-}2\text{-BF}_4\cdot 0.5\text{MeOH}$, $i\text{-}2\text{-B}(\text{C}_6\text{F}_5)_4$, $o\text{-}1\text{-BF}_4\cdot \text{CHCl}_3$, and $o\text{-}1\text{-B}(\text{C}_6\text{F}_5)_4\cdot 1.5\text{hexane}$.

In the case of $o\text{-}1\text{-BF}_4\cdot \text{CHCl}_3$, the copper center is surrounded by the coordinating nitrogen atoms, a bulky diphosphine moiety, and a BF_4^- ion. The interaction of the BF_4^- ion with the copper center in $o\text{-}2\text{-BF}_4\cdot 0.5\text{MeOH}$ is significantly stronger than in $o\text{-}1\text{-BF}_4\cdot \text{CHCl}_3$, considering the Cu-B distance. These results reflect the reduced bulkiness of dppp, owing to the presence of fewer phenyl groups, compared with DPEphos. In contrast, the methyl group in $i\text{-}2\text{-B}(\text{C}_6\text{F}_5)_4$ is located nearer to the copper atom rather than the counter anion. $\text{B}(\text{C}_6\text{F}_5)_4^-$ is distant from the copper center owing to a large steric repulsion between $\text{B}(\text{C}_6\text{F}_5)_4^-$ and the complex cation. Because of a similar coordination geometry to $o\text{-}2\text{-BF}_4\cdot 0.5\text{MeOH}$, the proximity of the counterion is seemingly the primary cause for destabilization in the i -isomer. On the other hand, the methyl group did not cover the copper center in $o\text{-}1\text{-B}(\text{C}_6\text{F}_5)_4\cdot 1.5\text{hexane}$, which is similar to $o\text{-}1\text{-BF}_4\cdot \text{CHCl}_3$. The results suggest that the position of the counterion has a small effect on the orientation of pyrimidine in 1^+ , due most likely to the bulkiness of the diphosphine moiety. As a

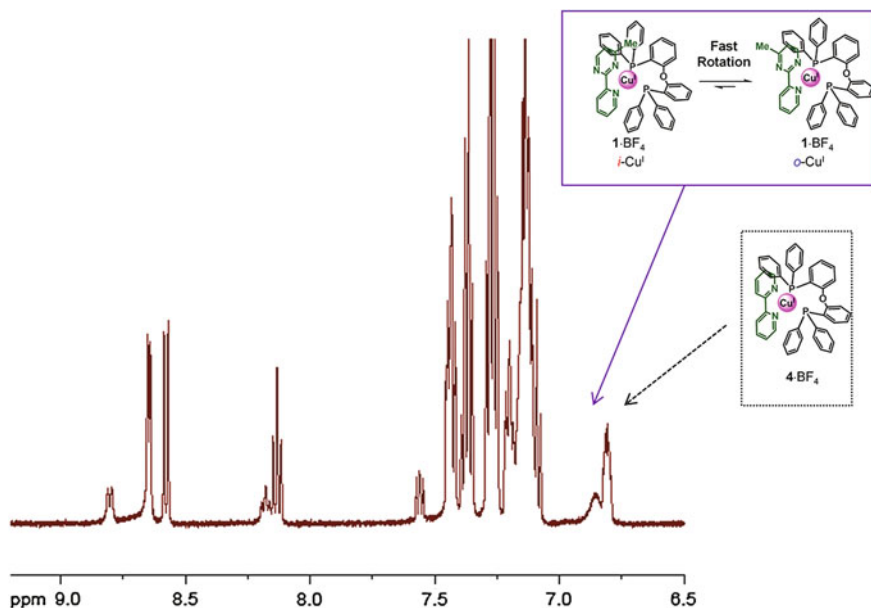


Fig. 2.15 Experimental ^1H NMR spectra of a mixture of $\mathbf{1}\text{-BF}_4$ and $\mathbf{4}\text{-BF}_4$ (bottom) in $\text{acetone-}d_6$ in the dark at 313 K. Representative signals of $\mathbf{1}\text{-BF}_4$ and $\mathbf{4}\text{-BF}_4$ are depicted by arrows. Since the rotation of $\mathbf{1}\text{-BF}_4$ is fast, a fusion of the signals derived from two isomers are observed. As the interconversion between $\mathbf{1}\text{-BF}_4$ and $\mathbf{4}\text{-BF}_4$ is very slow, the signals of $\mathbf{4}\text{-BF}_4$ are clearly resolved

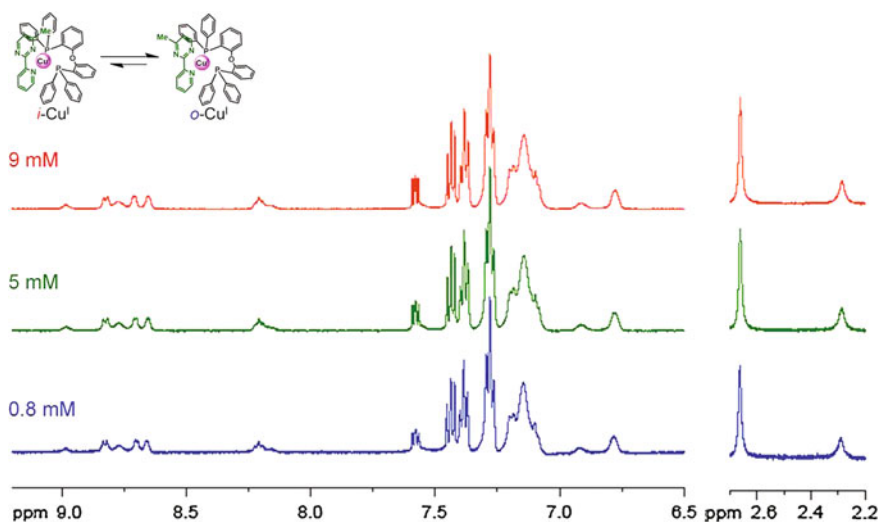


Fig. 2.16 Experimental ^1H NMR spectra of $\mathbf{1}\text{-BF}_4$ in $\text{acetone-}d_6$ at room temperature. Concentrations of $\mathbf{1}\text{-BF}_4$ are 9, 5, and 0.8 mM

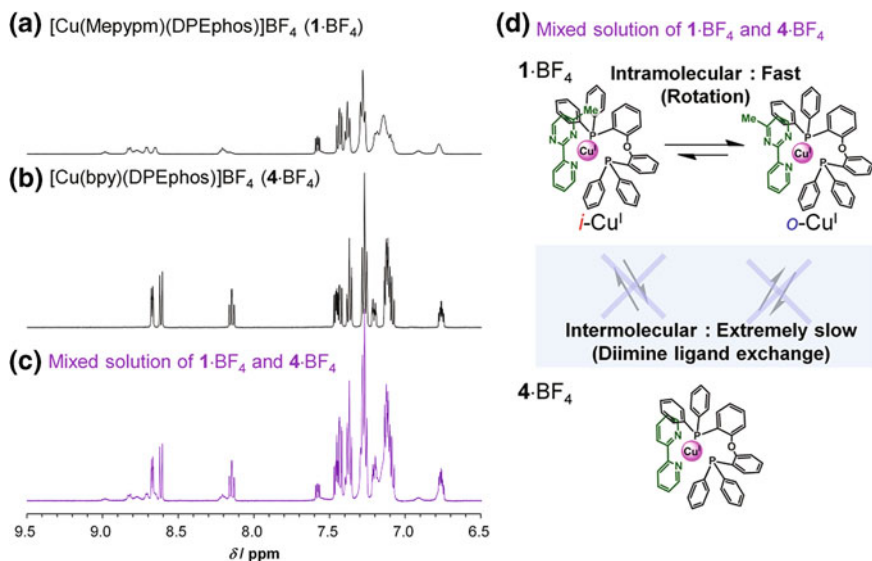


Fig. 2.17 a–c Partial ^1H NMR spectra of 2-BF_4 (a), 1-BF_4 (b), and a mixture of 1-BF_4 and 2-BF_4 (c) in acetone- d_6 in the dark at room temperature. d Illustration of the interconversion between species in a mixed solution of 1-BF_4 and 2-BF_4

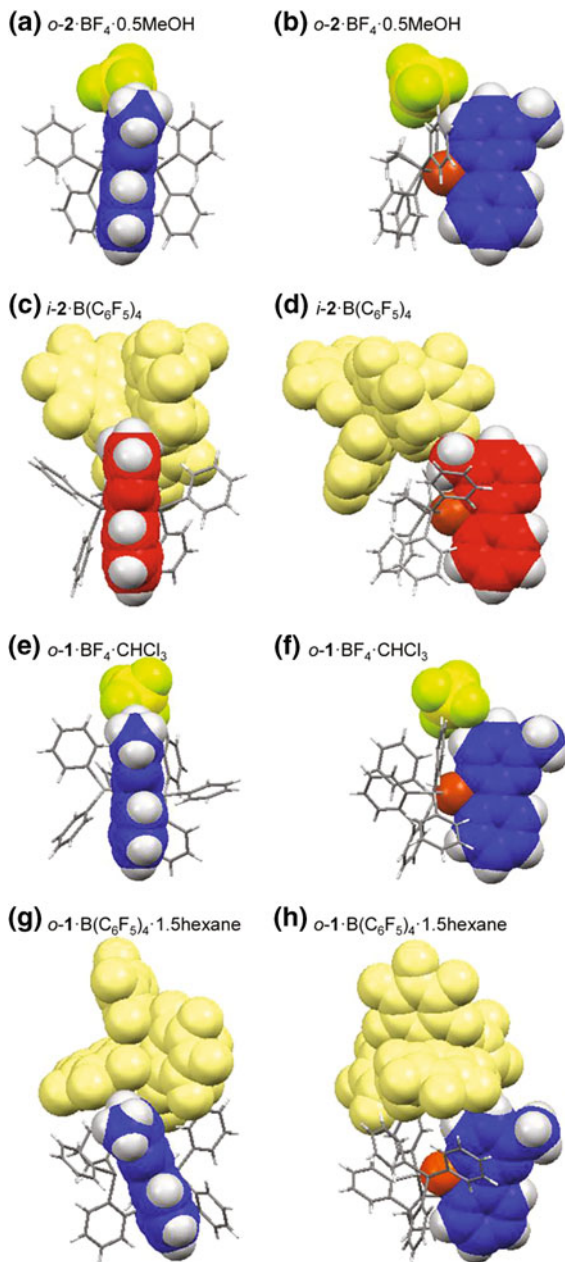
result, the effects of the counterion on the rotational dynamics of 2^+ are expected to be more significant than those operative in 1^+ . The aforementioned trend is characteristic of the $[\text{Cu}(\text{Mepypm})(\text{diphosphine})]^+$ family because of the geometry of the diphosphine ligand. Such behavior was not observed when bulky diimines were employed as the auxiliary ligand, such as in $[\text{Cu}(\text{Mepypm})(\text{L}_{\text{Anth}})]^+$ [37]. Examination of the crystal packing in the presented complexes reveals that the proximity of other species, such as solvent molecules or another complex salt, was less than that of the nearest counterion described above (Figs. 2.20, 2.21, 2.22, 2.23). The obtained crystal structures enable us to effectively construct a reasonable model for the sensitivity of rotational equilibrium on a weak-interaction in a solution state, which is described in the following section.

2.6 Thermodynamics of Rotation in Solution

2.6.1 Results

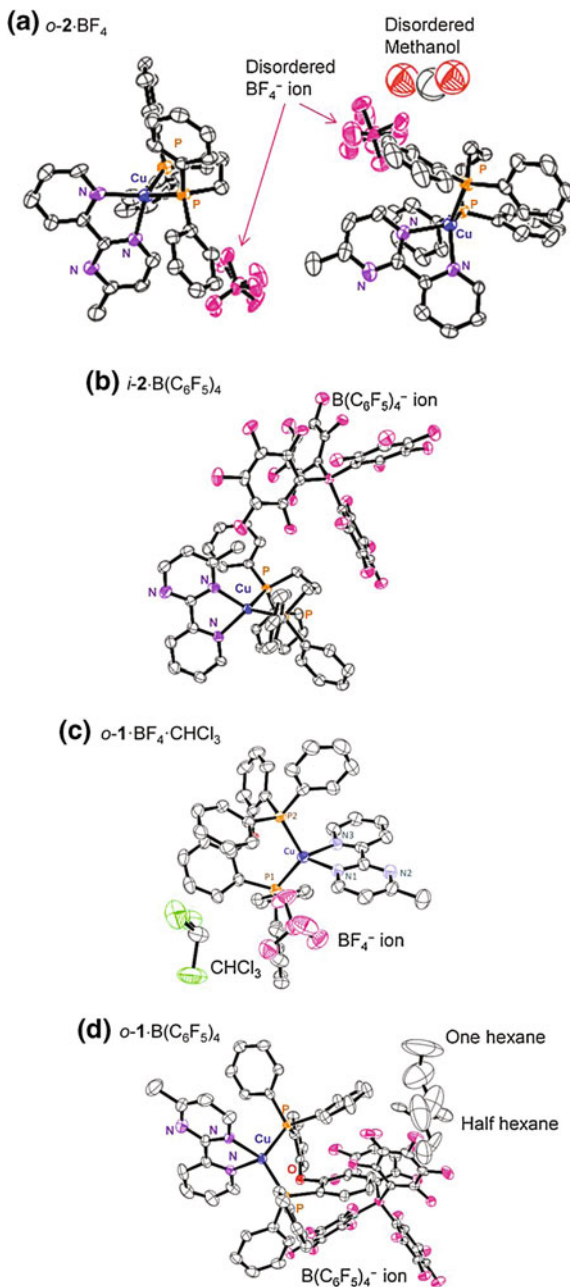
The thermodynamics of the rotational equilibrium of 1-BF_4 , $1\text{-B}(\text{C}_6\text{F}_5)_4$, 2-BF_4 , and $2\text{-B}(\text{C}_6\text{F}_5)_4$ was examined. The values of enthalpy (ΔH), entropy (ΔS), and Gibbs free energy (ΔG) for the $i\text{-Cu}^{\text{I}} \rightarrow o\text{-Cu}^{\text{I}}$ rotation were obtained using van't Hoff plots that were estimated from integration of the ^1H NMR spectra at various

Fig. 2.18 Front (a, c, e, g) and side (b, d, f, h) views of the crystal structures of *o*-2-BF₄·0.5MeOH (a, b), *i*-2-B(C₆F₅)₄ (c, d), *o*-1-BF₄·CHCl₃ (e, f), and *o*-1-B(C₆F₅)₄·1.5hexane (g, h). The carbon atoms in the Mepypm moiety are colored as blue or red, which correspond to *o*- and *i*-isomers, respectively. The Mepypm moiety, the copper atom, and the counterion are drawn as a space-filling model, whereas the diprophine moiety is included as a capped stick model. For clarity, some molecules are omitted: a, b a complex cation, a BF₄[−] ion, and a methanol molecule, e, f a chloroform molecule, g, h hexane molecules



temperatures in different solvents (Fig. 2.24). A negative ΔG corresponds to a predominance of the *o*-Cu^I compared with the *i*-Cu^I; In this case, the ratio of *o*-Cu^I, $x_o = [o\text{-Cu}^I]/([o\text{-Cu}^I] + [i\text{-Cu}^I])$, is more than 50 %, and equilibrium constant,

Fig. 2.19 ORTEP views of *o*-2·BF₄·0.5MeOH (a), *i*-2·B(C₆F₅)₄ (b), *o*-1·BF₄·CHCl₃ (c), and *o*-1·B(C₆F₅)₄·1.5hexane (d). The displacement ellipsoids are drawn at 50 % probability level. H atoms are omitted for clarity



$K = [o\text{-Cu}^{\text{I}}]/[i\text{-Cu}^{\text{I}}]$, is more than 1. A positive ΔH value corresponds to an enthalpic stabilization of *i*-Cu^I and a positive ΔS value to an entropic stabilization of *o*-Cu^I. The significant heat-sensitivity of the isomer ratios (Fig. 2.3) indicated

Fig. 2.20 Crystal structure of *o*-**2**·BF₄·0.5MeOH viewed along a-axis (a), b-axis (b), and c-axis (c). The Mepypm moiety, the copper atom and the BF₄[−] ion are drawn as a space filling model, whereas the diphosphine moiety as a capped stick model

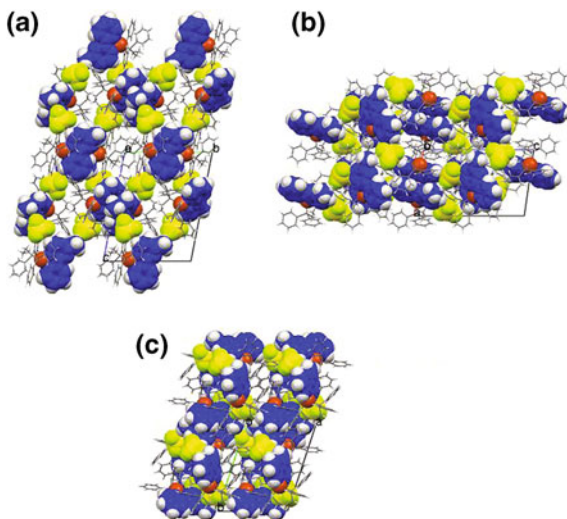
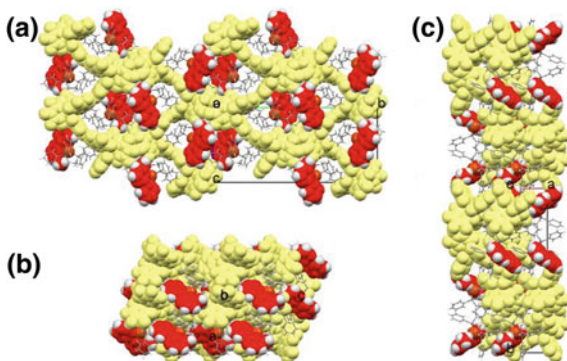


Fig. 2.21 Crystal structure of *i*-**2**·B(C₆F₅)₄ viewed along a-axis (a), b-axis (b), and c-axis (c). The Mepypm moiety, the copper atom and the BF₄[−] ion are drawn as a space filling model, whereas the diphosphine moiety as a capped stick model



the large value of ΔH . I denote ΔG , x_o , and K at 298 K as ΔG_{298} , x_{o298} , and K_{298} , respectively, and those at 233 K as ΔG_{233} , x_{o233} , and K_{233} , respectively. Selected parameters are tabulated in Table 2.3.

The results reveal two key points: (a) the values of both ΔH and ΔS of **2**·BF₄ in CDCl₃ were large and positive, and (b) the values of x_{298} were reduced in more polar solvents or by making use of a larger counterion.

The values of ΔH and ΔS of **1**·BF₄ in CDCl₃, CD₂Cl₂, acetone-*d*₆, CD₃CN, and **1**·B(C₆F₅)₄ in CDCl₃ fell within a range of 0–1 kJ mol^{−1} and 6–11 J K^{−1} mol^{−1}, respectively. In contrast, both the enthalpy and entropy values for the rotation of **2**·BF₄ in CDCl₃ ($\Delta H = 6$ kJ mol^{−1}, $\Delta S = 25$ J K^{−1} mol^{−1}) were more positive than that tested under other conditions (Table 2.3), such as in more polar solvents CD₂Cl₂ ($\Delta H = 4$ kJ mol^{−1}, $\Delta S = 15$ J K^{−1} mol^{−1}), acetone-*d*₆ ($\Delta H = 3$ kJ mol^{−1}, $\Delta S = 10$ J K^{−1} mol^{−1}), and CD₃CN ($\Delta H = 3$ kJ mol^{−1}, $\Delta S = 10$ J K^{−1} mol^{−1}).

Fig. 2.22 Crystal structure of *o*-**1**·BF₄·CHCl₃ viewed along a-axis (a), b-axis (b), and c-axis (c). The Mepypm moiety, the copper atom and the BF₄⁻ ion are drawn as a space filling model, whereas the diphosphine moiety as a capped stick model

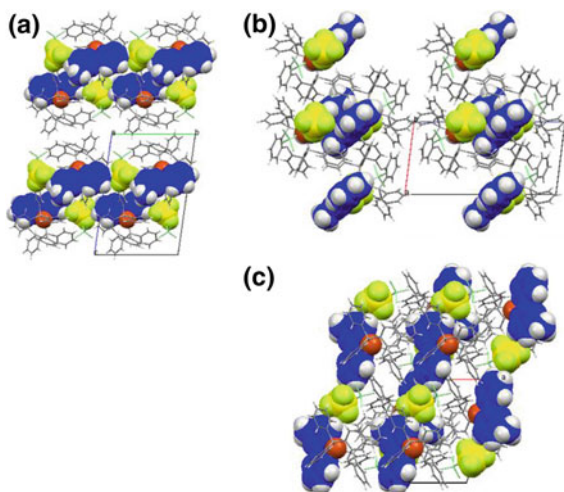
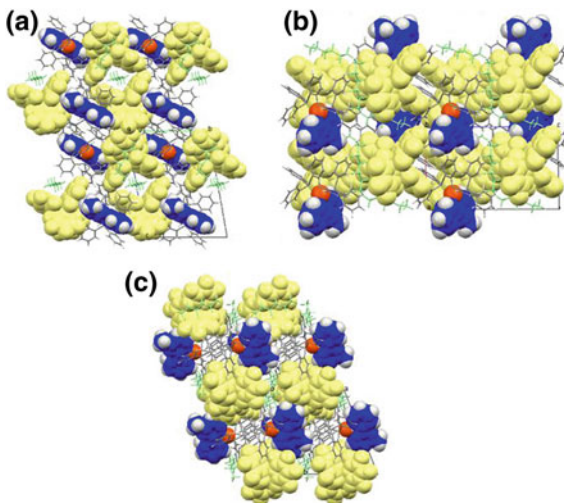


Fig. 2.23 Crystal structure of *o*-**1**·B(C₆F₅)₄·1.5hexane viewed along a-axis (a), b-axis (b), and c-axis (c). The Mepypm moiety, the copper atom and the BF₄⁻ ion are drawn as a space filling model, whereas the diphosphine moiety as a capped stick model



The parameters of *o*-**2**·B(C₆F₅)₄ in CDCl₃ ($\Delta H = 3 \text{ kJ mol}^{-1}$, $\Delta S = 13 \text{ J K}^{-1} \text{ mol}^{-1}$) were more negative than those of *o*-**2**·BF₄, indicating that the solvent and counterion effects on the values of both ΔH and ΔS of **1**⁺ were less than those of **2**⁺. In all tests, the values of ΔH and ΔS of **2**⁺, particularly ΔH , were more positive than those of **1**⁺. These results suggest that the diphosphine moieties considerably affect the enthalpy and entropy for the rotational isomerization.

A lower population of the *o*-Cu^I, which corresponds to a higher value of x_o , was found in the polar solvent. The values of x_{o298} of *o*-**1**·BF₄ were 74 % in CDCl₃, 70 % in CD₂Cl₂, 70 % in acetone-*d*₆, and 65 % in CD₃CN. This trend was found not only for *o*-**1**·BF₄ but also for *o*-**2**·BF₄. The values of x_{o298} for *o*-**2**·BF₄ in CD₂Cl₂,

Table 2.2 Selected bond lengths (Å), bond angles (°), a dihedral angle (°), a torsion angle (°) of *o*-1·BF₄·CHCl₃, *o*-1·B(C₆F₅)₄·1.5hexane, *o*-2·BF₄·0.5MeOH, and *i*-2·B(C₆F₅)₄

	<i>o</i> -1·BF ₄ ·CHCl ₃	<i>o</i> -1·B(C ₆ F ₅) ₄ ·1.5hexane	<i>o</i> -2·BF ₄ ·0.5MeOH	<i>i</i> -2·B(C ₆ F ₅) ₄
Cu–N _{pm} ^a /Å	2.061(5)	2.062(4)	2.059(5) 2.063(5)	2.070(3)
Cu–N _{py} ^b /Å	2.068(4)	2.092(4)	2.051(5) 2.048(5)	2.079(3)
Cu–P(1)/Å	2.2394(16)	2.2336(15)	2.2267(18) 2.2249(18)	2.2453(9)
Cu–P(2)/Å	2.2675(16)	2.2731(15)	2.2463(19) 2.246(2)	2.2561(9)
N–Cu–N/°	81.09(18)	80.24(17)	80.7(2) 80.6(2)	79.73(10)
P–Cu–P/°	114.37(5)	114.88(6)	103.45(7) 103.79(7)	102.06(3)
Dihedral angle/°	87.21	79.04	86.6 87.96	86.22
Torsion angle/°	9.07	17.36	4.01 6.24	5.4

^a A nitrogen atom of pyrimidine coordinating to a copper center^b A nitrogen atom of pyridine^c A dihedral angle between a N–Cu–N plane and a P–Cu–P plane^d A torsion angle between a pyrimidine plane and a pyridine plane

acetone-*d*₆, and CD₃CN were 56, 53, and 58 %, respectively, which are less than the values obtained in CDCl₃ (68 %). A lower population of the *o*-Cu^I, particularly in **2**⁺, was observed when a larger counterion was employed. The *x*_{o298} values of **2**·BF₄ and **2**·B(C₆F₅)₄ in CDCl₃ were 68 and 57 %, respectively. Significant counterion effects were not observed in **1**⁺; the ratio of **1**·B(C₆F₅)₄ in CDCl₃ (*x*_{o298} = 71 %) is slightly less than that of **1**·BF₄ in CDCl₃ (*x*_{o298} = 74 %). These trends are approximately observed in the full temperature range (see the van't Hoff plots in Fig. 2.24). The values of *x*_o of **1**⁺ under the conditions as we tested are almost constant over a temperature range from 233 K to 298 K. The heat-sensitivities of **2**⁺ are much larger than those of **1**⁺. For example, the population of the entropically favored *o*-Cu^I of **2**⁺ in CDCl₃ at 233 K is reduced at lower temperature (*x*_o = 54 %, Δ*G* = −0.3 kJ mol^{−1}). Because the values of Δ*H* under the other conditions were relatively small, the temperature dependence of *x*_o and Δ*G* were less significant than for **2**·BF₄ in CDCl₃.

The parameters Δ*H*, Δ*S*, Δ*G*₂₉₈, and *x*_{o298} were plotted against the Kirkwood function [1], (ε_r − 1)/(2ε_r + 1), where ε_r corresponds to the relative permittivity of the solvent (Fig. 2.25, ε_r = 4.89 for CDCl₃, 8.93 for CD₂Cl₂, 20.56 for acetone-*d*₆, and 35.94 for CD₃CN). Roughly linear relationships between the parameters and (ε_r − 1)/(2ε_r + 1) indicate that solvent polarity contributes considerably to the thermodynamics of the systems considered. The slopes of the four **2**·BF₄ plots, based on a linear least square regression fitting, were much larger than those of **1**·BF₄, suggesting that **2**⁺ is more sensitive to solvent selection than **1**⁺. The

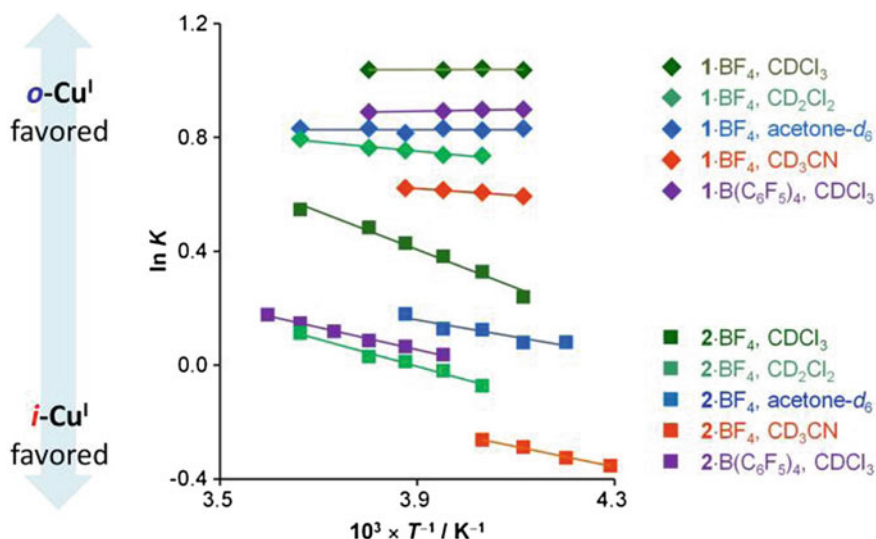


Fig. 2.24 van't Hoff plots for rotational equilibrium with the equilibrium constant, K , set equal to $[o\text{-isomer}]/[i\text{-isomer}]$

slopes of ΔG_{298} for both **1**-BF₄ and **2**-BF₄ are positive, indicating that the mechanism of the solvent dependency is similar throughout the [Cu(Me-pypm)(diphosphine)]⁺ family. There seems to be almost no relationship between ΔG_{298} and coordination ability of solvents (negligible donating ability for CDCl₃ and CD₂Cl₂, 17 for acetone-*d*₆, and 14.1 for CD₃CN) [1].

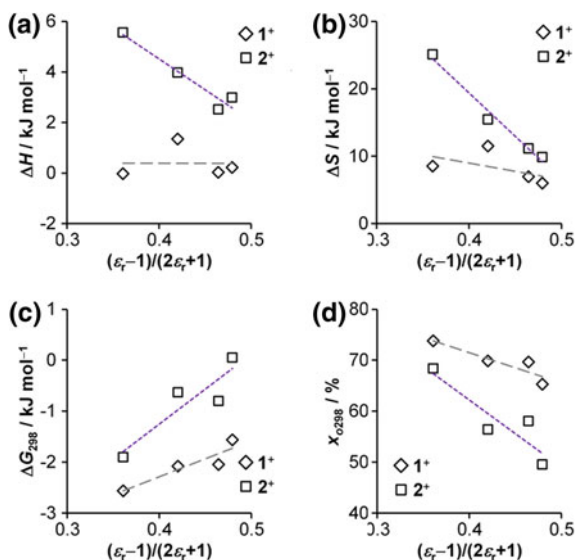
The aforementioned weak interaction dependence of the parameters ΔH , ΔS , ΔG_{298} , and x_{o298} cannot be explained by simple consideration of chemical structures alone. For completeness, with the aid generated crystal structures, I constructed a model that considers the geometries of both the ion pair and the six-membered chelating dppp moiety, as highlighted in the following section.

2.6.2 Discussion

The geometric features of **1**⁺ and **2**⁺ are illustrated at Fig. 2.26a. The major bonding surface of the copper center in both **1**⁺ and **2**⁺ is occupied by the coordinating nitrogen atoms and the diphosphine moiety. The bonding area taken up by coordination in **2**⁺ is reduced compared with that in **1**⁺, which provides additional space that a counterion or a methyl group on the pyrimidine moiety can occupy. Contributions of the CIP state in CDCl₃ are larger than in more polar solvents such as CD₃CN (Fig. 2.26b) [1]. In other words, the population of the SSIP state in polar solvent is larger than that in less polar solvent. For clarity, I focus on the

Table 2.3 Selected thermodynamic parameters for the rotational equilibrium of [Cu(Me-pym)(diphosphine)]⁺ complexes under various conditions

	Solvent	ΔH^a	ΔS^b	ΔG_{298}^c	x_{o298}^e	K_{298}^g	ΔG_{233}^d	x_{o233}^f	K_{233}^h
1·BF ₄	CDCl ₃	0.0	8	−2.6	74	2.8	−2.0	74	2.8
1·BF ₄	CD ₂ Cl ₂	1.3	11	−2.1	70	2.3	−1.3	67	2.0
1·BF ₄	Acetone- <i>d</i> ₆	0.0	7	−2.1	70	2.3	−1.6	70	2.3
1·BF ₄	CD ₃ CN	0.2	6	−1.6	65	1.9	−1.2	65	1.8
1·B(C ₆ F ₅) ₄	CDCl ₃	−0.2	6	−2.2	71	2.4	−1.7	71	2.5
2·BF ₄	CDCl ₃	5.6	25	−1.9	68	2.2	−0.3	54	1.2
2·BF ₄	CD ₂ Cl ₂	4.0	15	−0.6	56	1.3	0.4	45	0.8
2·BF ₄	Acetone- <i>d</i> ₆	2.5	10	−0.3	58	1.4	−0.1	51	1.0
2·BF ₄	CD ₃ CN	3.0	10	0.0	50	1.0	0.7	41	0.7
2·B(C ₆ F ₅) ₄	CDCl ₃	3.3	13	−0.7	57	1.3	0.2	48	0.9

^a Enthalpy for *i*-Cu^I → *o*-Cu^I rotation/kJ mol^{−1}^b Entropy for *i*-Cu^I → *o*-Cu^I rotation/J K^{−1} mol^{−1}^{c,d} Gibbs free energy for *i*-Cu^I → *o*-Cu^I rotation at ^c 298 K and ^d 233 K/kJ mol^{−1}^{e,f} Molar ratio of *o*-Cu^I at ^e 298 K and ^f 233 K/ %^{g,h} Equilibrium constant, [*o*-Cu^I]/[*i*-Cu^I] at ^g 298 K and ^h 233 K**Fig. 2.25** Correlation between the Kirkwood function, $(\epsilon_r - 1)/(2\epsilon_r + 1)$, and thermodynamic parameters, ΔH (a), ΔS (b), ΔG_{298} (c), and x_{o298} (d), of 1·BF₄ and 2·BF₄ in CDCl₃, CD₂Cl₂, acetone-*d*₆, and CD₃CN

representative two ion-pairing states, and omit the others. It should be noted that ion pairing between a monovalent metal complex cation and a monovalent counter anion is strengthened in CDCl₃, moderate in CD₂Cl₂, and weakened in more polar solvent such as acetone-*d*₆, reported by several groups [2–6]. On the other hand, with respect to the size of the anion, BF₄[−] is significantly smaller than B(C₆F₅)₄[−], which is comparable with the size of the copper complex cation.

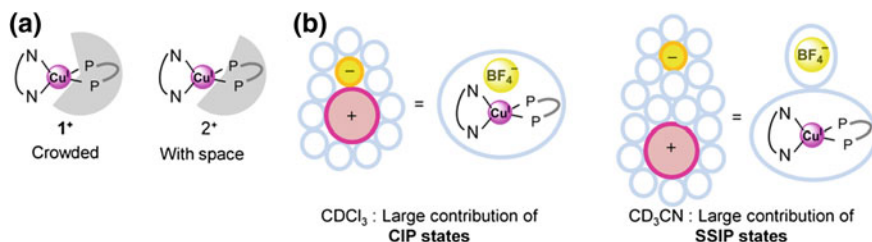


Fig. 2.26 Illustrations of the effect of ion pairing on the rotational bistability of a [Cu(Mepypm)(diphosphine)]⁺ family. **a** Geometric features of the diphosphine moieties of **1**⁺ and **2**⁺. **b** The Cu(I) complexes in a contact ion pair (CIP) state and a solvent-separated ion pair (SSIP) state

The value of ΔH for solvated *i*-Cu^I and *o*-Cu^I is linked to intrinsic preference caused by induction effect of the methyl group, electrostatic interactions, solvation, electrostatic attraction between the electron cloud of the methyl group and the positively charged metal core of the complex, and other enthalpic factors present. The ΔS values are a reflection of their respective freedom of rotation of functional groups, along with the vibrational freedom of the ligand moieties, the solvent, and the counterion. For example, the large positive values of **2**·BF₄ in CDCl₃ indicate that the behavior of the solvated *i*-Cu^I differs significantly from the solvated *o*-Cu^I. In addition, the relatively small absolute values of both ΔH and ΔS of other conditions, **2**·BF₄ in polar solvent, **1**·BF₄ in all solvents as we tested, **2**·B(C₆F₅)₄ in CDCl₃, and **1**·B(C₆F₅)₄ in CDCl₃, indicate that the differences in the behaviors between the solvated *i*- and *o*-isomers are trivial.

The rotational equilibrium in solution is represented as a model, displayed in Fig. 2.27. Six conditions are represented: (a) **2**·BF₄ in CDCl₃, (b) **2**·BF₄ in CD₃CN, (c) **2**·B(C₆F₅)₄ in CDCl₃, (d) **1**·BF₄ in CDCl₃, (e) **1**·BF₄ in CD₃CN, and (f) **1**·B(C₆F₅)₄ in CDCl₃. The equilibrium behaviors in CD₂Cl₂ and acetone-*d*₆ can be interpreted as a range from those in less polar CDCl₃ to those in more polar CD₃CN, considering their moderate thermodynamic parameters and relative permittivity. Each result has two points: (i) ΔH and ΔS , (ii) ΔG_{298} and x_{o298} .

The six conditions a–f are explained as follows. (a-i) The values of ΔH and ΔS of **2**·BF₄ in CDCl₃ are larger in magnitude and more positive than those under other conditions. In the CIP state of solvated *o*-Cu^I, there are no steric repulsion between the counterion and the methyl group (Fig. 2.27a). In contrast, the CIP state of the solvated *i*-Cu^I competes for the counterion, BF₄⁻, and the methyl group on the pyrimidine unit as a result of steric repulsion. This repulsion can be correlated to destabilization of the solvated *i*-Cu^I, which corresponds to more positive values of ΔS , owing to loss of freedom in the complex cation as well as the counterion. The larger difference in solvation between *i*-Cu^I and *o*-Cu^I can cause more positive ΔH . Enhanced solvated *i*-Cu^I preference based on a combination of several enthalpic factors described above can contribute to ΔH because its movement is strongly limited by the competition. (a-ii) The negative value of

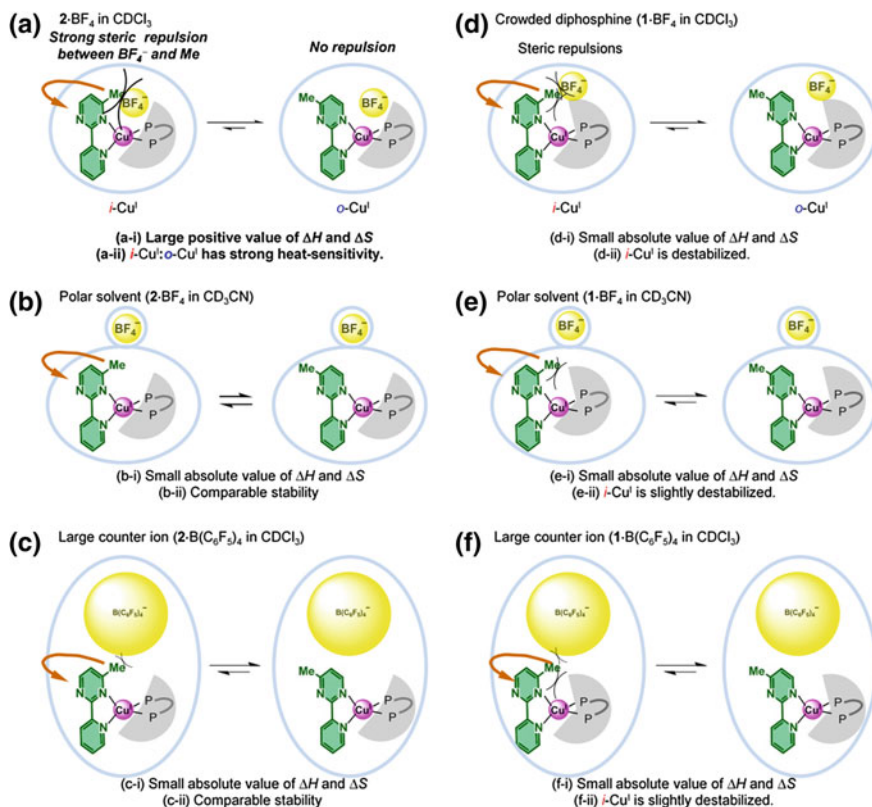


Fig. 2.27 Illustrations of the effect of ion pairing on the rotational bistability of a $[\text{Cu}(\text{Meypym})(\text{diphosphine})]^+$ family. Selected chemical equilibrium between the solvated i - and o -isomers: **a** 2-BF_4 in CDCl_3 , **b** 2-BF_4 in CD_3CN , **c** $2\text{-B}(\text{C}_6\text{F}_5)_4$ in CDCl_3 , **d** 1-BF_4 in CDCl_3 , **e** 1-BF_4 in CD_3CN , and **f** $1\text{-B}(\text{C}_6\text{F}_5)_4$ in CDCl_3

ΔG_{298} indicates that the population of the entropically-favorable solvated $o\text{-Cu}^I$, mentioned in (a-i), is larger than that of $i\text{-Cu}^I$ at 298 K. At low temperature such as 233 K, where the entropic factor is less dominant, both isomers have comparable stability; absolute value of ΔG_{233} is nearly zero. The comparable stabilization effects in the viewpoint of enthalpy and entropy cause the rotational bistability.

(b-i) The effects of solvent polarity are described in this paragraph. The ΔH and ΔS of 2-BF_4 are positively small in polar solvents such as CD_3CN (Fig. 2.27b). The steric repulsion between the methyl group on the pyrimidine moiety and the counterion, mentioned in paragraph (a-i), is relatively small in theSSIP states of both the solvated $i\text{-Cu}^I$ and $o\text{-Cu}^I$. Because difference in solvation between $i\text{-Cu}^I$ and $o\text{-Cu}^I$ is relatively small, the absolute values of ΔH and ΔS are also small. (b-ii) The x_{o298} values of 2-BF_4 in CD_3CN are smaller than in CDCl_3 because the destabilization of the solvated $i\text{-Cu}^I$, mentioned in paragraph (a), is considerably

minimized in the SSIP state. The more positive value of ΔG_{298} in CD_3CN compared to that in CDCl_3 also reflects this trend.

(c-i) The effects of the counterion size are explained in this paragraph. The ΔH and ΔS of $2\cdot\text{B}(\text{C}_6\text{F}_5)_4$ in CDCl_3 are more negative than those of $2\cdot\text{BF}_4$ in CDCl_3 (Fig. 2.27c). Because the $\text{B}(\text{C}_6\text{F}_5)_4^-$ ion causes a small destabilization of the $i\text{-Cu}^{\text{I}}$ in the CIP state, as described in paragraph (a), derived from its size, the small difference in solvation between two isomers contributes to small absolute values of ΔH and ΔS . (c-ii) The inhibition of the destabilization of the $i\text{-Cu}^{\text{I}}$ also causes a decrease in x_{o298} for the $\text{B}(\text{C}_6\text{F}_5)_4^-$ ion compared with the BF_4^- ion; The more positive value of ΔG_{298} with $\text{B}(\text{C}_6\text{F}_5)_4^-$ ion compared to BF_4^- ion also reflects this trend.

(d-i) The effect of the geometry of the diphosphine ligand is described in paragraphs (d), (e), and (f). Despite the absolute values of ΔH and ΔS of $2\cdot\text{BF}_4$ in CDCl_3 being relatively large, those of $1\cdot\text{BF}_4$ in CDCl_3 are small since the bulkiness of the diphosphine of 1^+ reduces the steric repulsion between the methyl group of the solvated i -isomer and the counterion, as mentioned in (a-i) (Fig. 2.27d). The reason of nearly zero ΔH value of 1^+ can be interpreted as small difference in solvation between $i\text{-Cu}^{\text{I}}$ and $o\text{-Cu}^{\text{I}}$ (Fig. 2.27d). (d-ii) The value of ΔG_{298} is negative because the bulkiness of the diphosphine contributes to a destabilization of $i\text{-Cu}^{\text{I}}$ via steric repulsion between the methyl group and the diphosphine moiety. The bulkiness is also the reason why x_{o298} of $1\cdot\text{BF}_4$ in several solvents is larger than that of $2\cdot\text{BF}_4$.

(e-i) The absolute values of both ΔH and ΔS of $1\cdot\text{BF}_4$ in CD_3CN are small because of a combination of phenomena described in (b-i) and (d-i) (Fig. 2.27e). (e-ii) The negative ΔG stems from the steric bulk of the diphosphine as described in (d-ii). The lower x_{o298} of $1\cdot\text{BF}_4$ in polar solvents compared with $1\cdot\text{BF}_4$ in CDCl_3 was attributed to ion pairing effects, as highlighted in the above comparison of (a) and (b).

(f-i) The absolute values of both ΔH and ΔS of $1\cdot\text{B}(\text{C}_6\text{F}_5)_4$ in CDCl_3 are small due to a combination of (c-i) and (d-i) phenomena (Fig. 2.27f). (f-ii) Since the ion pairing effects are slightly retained, the x_{o298} of $1\cdot\text{B}(\text{C}_6\text{F}_5)_4$ was lower than that of $1\cdot\text{BF}_4$.

The values of both ΔH and ΔS contain a contribution of the effects mentioned above as well as the following intrinsic factors. Several factors can contribute to the values. For example, the stabilization of $i\text{-Cu}^{\text{I}}$ stemming from the electronic structure of Mepypm, which can be derived from induction effects, and thus contribute to positive ΔH values. A stabilization of $i\text{-Cu}^{\text{I}}$ caused by an easing of the C–H interaction between the methyl group and the phenyl groups on the diphosphine, can also contribute to positive ΔH values. The entropy loss of $i\text{-Cu}^{\text{I}}$ originates from a crowded coordination geometry, which reduces the freedom of motion of the ligand moiety, thus contributing to positive values of ΔS . These intrinsic factors also contribute to the values of x_o .

Consequently, all results related to thermodynamics can be reasonably understood based on the proposed model, suggesting that the present rotational bistability, particularly in 2^+ , arises from solvated ion-pairing.

2.6.3 Notes About the Model

I note that the ^1H NMR signals can be the average of many kinds of conformations, such as the solvent, the counterion, and the ligands including the diphosphine moiety. The conceptual diagrams, displayed in Fig. 2.27, are representative of the real equilibrium.

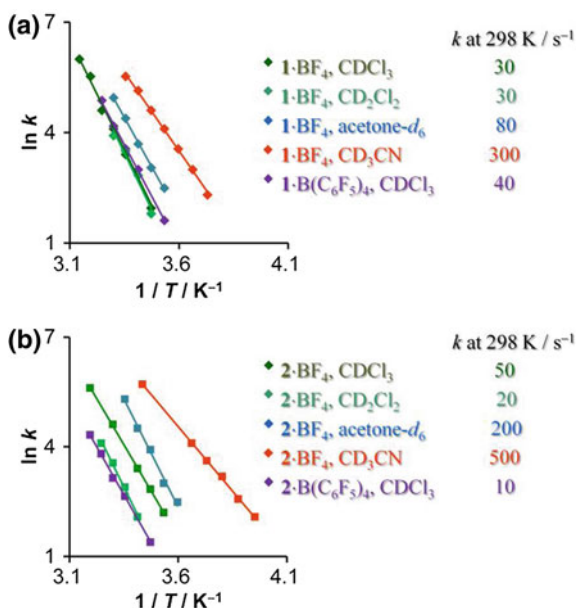
Since the crystal structures of a family of $[\text{Cu}(\text{Mepypm})(\text{diimine})]^+$ [37–40], including a complex in Chap. 4, were very different from those of the present complexes, particularly from the viewpoint of coordination structure and location of the counterion, the ion-pairing sensitivity derived from model mentioned above is characteristic of $[\text{Cu}(\text{Mepypm})(\text{diphosphine})]^+$ structures.

Changes in dipole moment, hydrogen bonding interaction, and hydrophobic interactions between two states are often attributed to solvent-sensitivity not only in traditional conformational equilibrium such as axial/equatorial forms in cyclohexane derivatives¹ but also in chemistry for promising nanomaterials such as molecular machines based on supramolecules [27–36]. Because the complex cations of the two isomers are similar with respect to coordination structure, the polarity differences between *i*-Cu^I and *o*-Cu^I are expected to be small. On the other hand, the absolute value of the dipole moment of the solvated copper(I) compounds is expected to be proportional to the distance between the copper atom and the counterion center (Cu-X). Therefore, the polarity of the *i*-isomer in the CIP state is expected to be larger than that of the *o*-isomer, considering that the Cu-X distance is determined by steric repulsion. This is an additional effect caused by ion pairing as described in Fig. 2.27. The difference in polarity between the two isomers in the CIP state can contribute to the preference of the *i*-Cu^I for more polar solvent. This rationale is incomplete for three reasons: (1) the population of the CIP state in polar solvent is small, (2) the difference of the Cu-X distance between *i*- and *o*-isomers in the SSIP state is small, and (3) the large ΔH and ΔS of $2 \cdot \text{BF}_4$ in CDCl_3 cannot be appropriately explained by this reasoning.

If a solvent molecule, such as CD_3CN which has high affinity to copper(I) state, coordinates to the copper(I) center of present complexes, steric repulsion between the methyl group and the solvent molecule would cause a decrease of *i*-Cu^I ratio in CD_3CN compared with CDCl_3 . This assumption can be totally denied, because of both experimental results and electronic configuration; The copper(I) center has already the coordination number of 4, so that it cannot accommodate any additional ligand.

I assume that the volume where BF_4^- ion is present, displayed in Fig. 2.27a, can be occupied by a CDCl_3 molecule instead of the counterion, which can destabilize *i*-Cu^I via steric repulsion between the methyl group and the solvent molecule. Since this assumption does not explain the decrease in the *o*-Cu^I molar ratio when a larger counterion is used, the effects of the size of the solvent molecule are small.

Fig. 2.28 The Arrhenius plots and the rate constant at 298 K for the $i\text{-Cu}^{\text{I}} \rightarrow o\text{-Cu}^{\text{I}}$ interconversion of 1^+ (a) and 2^+ (b) under a variety of conditions



2.7 Rate for the Isomerization in a Solution State

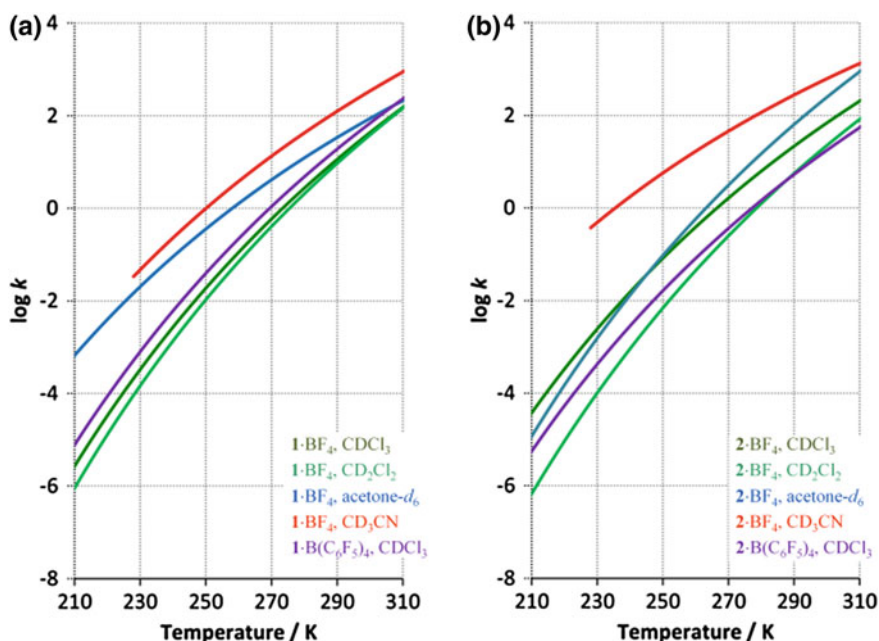
The rate constants for the $i\text{-Cu}^{\text{I}} \rightarrow o\text{-Cu}^{\text{I}}$ isomerization, k , at variable temperature were estimated from Arrhenius plots based on simulation of the broadened ^1H NMR spectra (Figs. 2.4, 2.5, 2.6, 2.7, 2.8, 2.9, 2.10, 2.11, 2.12, 2.13 and 2.28). The values of k at 298 K, k_{298} , which are the parameters most representative of the solvent- and counterion-sensitive kinetics, are also summarized in Fig. 2.28. Other parameters are tabulated in Table 2.4.

The kinetics analysis supports the validity of the thermodynamic analysis. The magnitude of the k values at the given temperature, where ^1H NMR spectra for the thermodynamic analysis were conducted, falls within a range from 10^{-2} to 10^0 s^{-1} (Fig. 2.29). Qualitatively, the values indicate that the system reaches equilibrium within 10^2 s . For the ^1H NMR spectra conducted with ca. 10^3 s intervals, the signal integrations reflect the ratio of $i\text{-Cu}^{\text{I}}$ and $o\text{-Cu}^{\text{I}}$ in equilibrium. Signal broadening is observed when k exceeds ca. 10^1 s^{-1} . The ^1H NMR spectra at high temperature are not employed for the thermodynamic analysis.

The much larger k_{298} values obtained in coordinating solvent such as CD_3CN , compared with non-coordinating solvent such as CDCl_3 , were observed not only for 1-BF_4 (30 s^{-1} in CDCl_3 , 30 s^{-1} in CD_2Cl_2 , 80 s^{-1} in acetone- d_6 , and 300 s^{-1} in CD_3CN) but also for 2-BF_4 (50 s^{-1} in CDCl_3 , 20 s^{-1} in CD_2Cl_2 , 200 s^{-1} in acetone- d_6 , and 500 s^{-1} in CD_3CN). The promotion of the isomerization by high affinity of coordination of a solvent molecule to copper(I) ion, which assists the dissociation of the pyrimidine nitrogen atoms from the copper center, was

Table 2.4 Selected kinetic parameters for the rotational equilibrium of a family of $[\text{Cu}(\text{Mepypm})(\text{diphosphine})]^+$ in several conditions

	Solvent	E_a^a	$\log(A)^b$	k_{298}^c
1·BF ₄	CDCl ₃	100	19	30
1·BF ₄	CD ₂ Cl ₂	100	19	30
1·BF ₄	Acetone-d ₆	70	14	80
1·BF ₄	CD ₃ CN	70	15	300
1·B(C ₆ F ₅) ₄	CDCl ₃	90	18	40
2·BF ₄	CDCl ₃	80	16	50
2·BF ₄	CD ₂ Cl ₂	100	19	20
2·BF ₄	Acetone-d ₆	100	19	200
2·BF ₄	CD ₃ CN	60	13	500
2·B(C ₆ F ₅) ₄	CDCl ₃	90	16	10

^a Activation energy for $i\text{-Cu}^I \rightarrow o\text{-Cu}^I$ rotation/kJ mol⁻¹^b Logarithm of frequency factor for $i\text{-Cu}^I \rightarrow o\text{-Cu}^I$ rotation^c Rate constant for $i\text{-Cu}^I \rightarrow o\text{-Cu}^I$ rotation at 298 K/s⁻¹**Fig. 2.29** The rate constants, k , for the $i\text{-Cu}^I \rightarrow o\text{-Cu}^I$ rotational isomerization of **1⁺** (a) and **2⁺** (b) in several conditions as a function of temperature, estimated from the Arrhenius plots. Regression curves of the Arrhenius plots are indicated by lines

generally found throughout the $[\text{Cu}(\text{Mepypm})(\text{diphosphine})]^+$ family. The value of k_{298} in a CDCl₃ solution of **2·B(C₆F₅)₄** is 10 s⁻¹, which is smaller than that of **2·BF₄**. The decrease of k_{298} resulting from the use of a bulky counter anion

suggests that the weak coordination ability of BF_4^- can slightly assist in Cu–N bond dissociation. This behavior seems to be consistent with the model describing the BF_4^- ion approach in the CIP state. $\mathbf{1}\cdot\text{B}(\text{C}_6\text{F}_5)_4$ in CDCl_3 ($k_{298} = 40 \text{ s}^{-1}$) is very similar to $\mathbf{1}\cdot\text{BF}_4$ in CDCl_3 . The resemblance also seems to relate to the model provided in Fig. 2.27. The rate constant associated with $\mathbf{1}\cdot\text{BF}_4$ in CD_2Cl_2 was comparable with that of $\mathbf{1}\cdot\text{BF}_4$ in CDCl_3 , because the coordination abilities of CD_2Cl_2 and CDCl_3 are similarly weak. In contrast, a small decrease of k_{298} in CD_2Cl_2 compared with CDCl_3 was observed for $\mathbf{2}\cdot\text{BF}_4$. The solvent sensitivity seems to be consistent with the model illustrating that the ion-pairing sensitivity of $\mathbf{2}^+$ is larger than that of $\mathbf{1}^+$, shown in Fig. 2.27. This result can be interpreted as a promotion of rotation by enhancement of coordination ability of BF_4^- ion in CIP state. These CIP effects can contribute to the kinetics of rotation, but this effect seems to be smaller than that of the solvent coordination.

A tricoordinated intermediate, where the nitrogen atom on the pyrimidine unit is dissociated from the copper center, is one of the possible intermediates. One of the another possible intermediates is a tetracoordinated intermediate, which is coordinated by one nitrogen atom on pyridine unit, two phosphine atoms, and one solvent molecule, because the rate of rotation in the coordinative solvent such as CD_3CN , which has high coordination affinity to copper center, is found to be much faster than that in the non-coordinative solvent such as CDCl_3 .

On the other hand, viscosity of CHCl_3 , CH_2Cl_2 , acetone, and CH_3CN is 0.5357, 0.449, 0.3029, and 0.341 cP, respectively. Rate constants for $i\text{-Cu}^{\text{I}} \rightarrow o\text{-Cu}^{\text{I}}$ at 298 K (k_{298}) in CDCl_3 , CD_2Cl_2 , acetone- d_6 , and CD_3CN are 50, 20, 200, and 500 s^{-1} , respectively (Table 2.4). Additionally, viscosity of CH_3OH is 0.5513, and k_{298} in CD_3OD is 150, estimated from preliminary experiment. Contribution of viscosity seems to be much smaller than that of coordination affinity to copper(I), because rate constants in CDCl_3 and CD_3OD , which have similar values of viscosity, are significantly different.

The solvent sensitivity trends, mentioned above, are basically observed over the full temperature range tested (see Arrhenius plots in Fig. 2.28). The k value varied from 10^{-6} (frozen motion) to 10^3 s^{-1} over the temperature and solvent ranges considered (Fig. 2.29).

2.8 Conclusion

A series of simple copper(I) complexes bearing a Mepypm and a diphosphine ligand, $[\text{Cu}(\text{Mepypm})(\text{diphosphine})]^+$, namely, $\mathbf{1}\cdot\text{BF}_4$, $\mathbf{1}\cdot\text{B}(\text{C}_6\text{F}_5)_4$, $\mathbf{2}\cdot\text{BF}_4$, and $\mathbf{2}\cdot\text{B}(\text{C}_6\text{F}_5)_4$ was synthesized. Two rotational isomers, $i\text{-Cu}^{\text{I}}$ and $o\text{-Cu}^{\text{I}}$, coexist and interconvert in solution via intramolecular ligating atom exchange of the pyrimidine ring in all complexes as I tested. The interconversion between $i\text{-Cu}^{\text{I}}$ and $o\text{-Cu}^{\text{I}}$ is generally an intramolecular process, as confirmed by ^1H NMR analysis of a mixed solution of $\mathbf{1}\cdot\text{BF}_4$ and $[\text{Cu}(\text{bpy})(\text{DPEphos})]\text{BF}_4$. Both the enthalpy and entropy values for $i\text{-Cu}^{\text{I}} \rightarrow o\text{-Cu}^{\text{I}}$ rotation of $\mathbf{2}\cdot\text{BF}_4$ in CDCl_3 ($\Delta H = 6 \text{ kJ mol}^{-1}$,

$\Delta S = 25 \text{ J K}^{-1} \text{ mol}^{-1}$) were larger than that tested under other conditions. The absolute values of both ΔH and ΔS significantly decreased in more polar solvents, such as CD_2Cl_2 , acetone- d_6 , and CD_3CN . The reduced contact of the counteranion to the complex cation in polar solvent contributes to the relative stability of the isomers: The values of $x_{o298} = [o\text{-Cu}^I]/([i\text{-Cu}^I] + [o\text{-Cu}^I])$ are 68 % (**2**- BF_4 in CDCl_3), 50 % (**2**- BF_4 in CD_3CN), 74 % (**1**- BF_4 in CDCl_3), and 65 % (**1**- BF_4 in CD_3CN). This speculation based on solvated ion pairing was further confirmed by considering the rotation behavior with a bulky counterion, $\text{B}(\text{C}_6\text{F}_5)_4^-$. Crystal structures of $o\text{-Cu}^I$ (**1**- BF_4 , **1**- $\text{B}(\text{C}_6\text{F}_5)_4$ and **2**- BF_4) and $i\text{-Cu}^I$ (**2**- $\text{B}(\text{C}_6\text{F}_5)_4$) are helpful to construct the model. The findings described herein are valuable for the design of photo- and/or redox-active molecular mechanical units that can be readily functionalized via weak electrostatic interactions. The rate constants for interconversion between $i\text{-Cu}^I$ and $o\text{-Cu}^I$ varied from 10^{-6} (frozen motion) to 10^3 s^{-1} over the temperature and solvent ranges considered.

The slow rate of rotation plays a key role for functions of our rotational system. For example, in the previous report, we have developed switching systems by trapping metastable states. This strategy enables me to construct PET-driven rotation system, described in [Chap. 4](#). For another example, I have demonstrated dual emission caused by ring rotational isomerization, described in [Chap. 3](#). Common organic solution state is found to be suitable for these desired functions.

References

1. Reichardt C (2003) Solvents and solvent effects in organic chemistry, 3rd edn. Wiley-VCH, Weinheim
2. Macchioni A (2005) Chem Rev 105:2039–2073
3. Moreno A, Pregosin PS, Veiros LF, Albinati A, Rizzato S (2009) Chem Eur J 15:6848–6862
4. Kumar PGA, Pregosin PS, Goicoechea JM, Whittlesey MK (2003) Organometallics 22:2956–2960
5. Pregosin PS, Kumar PGA, Fernández I (2005) Chem Rev 105:2977–2998
6. Martinez-Viviente E, Pregosin PS (2003) Inorg Chem 42:2209–2214
7. Lacour J, Moraleda D (2009) Chem Commun 7073–7089
8. Hebbe-Viton V, Desvergues V, Jodry JJ, Dietrich-Buchecker C, Sauvage J-P, Lacour J (2006) Dalton Trans 2058–2065
9. Desvergues-Breuil V, Hebbe V, Dietrich-Buchecker C, Sauvage J-P, Lacour J (2003) Inorg Chem 42:255–257
10. Hutin M, Nitschke JR (2006) Chem Commun 1724–1726
11. Merrill CL, Wilson LJ, Thamann TJ, Loehr TM, Ferris NS, Woodruff WH (1984) J Chem Soc Dalton Trans 2207–2221
12. Liang H-C, Kim E, Incarvito CD, Rheingold AL, Karlin KD (2002) Inorg Chem 41:2209–2212
13. Letko CS, Rauchfuss TB, Zhou X, Gray DL (2012) Inorg Chem 51:4511–4520
14. Lee Y, Lee D-H, Park GY, Lucas HR, Narducci Sarjeant AA, Kieber-Emmons MT, Vance MA, Milligan AE, Solomon EI, Karlin KD (2010) Inorg Chem 49:8873–8885
15. Medwid JB, Paul R, Baker JS, Brockman JA, Du MT, Hallett WA, Hanifin JW, Hardy RA, Tarrant ME, Torley LW, Wrenn S (1990) J Med Chem 33:1230–1241
16. Lafferty JJ, Case FH (1967) J Org Chem 32:1591–1596

17. Kuang SM, Cuttell DG, McMillin DR, Fanwick PE, Walton RA (2002) *Inorg Chem* 41:3313–3322
18. Saito K, Arai T, Takahashi N, Tsukuda T, Tsubomura T (2006) *Dalton Trans* 4444–4448
19. Yang L, Feng JK, Ren AM, Zhang M, Ma YG, Liu XD (2005) *Eur J Inorg Chem* 1867–1879
20. Altomare A, Cascarano G, Giacovazzo C, Guagliardi A, Burla MC, Polidori G, Camalli M (1994) *J Appl Cryst* 27:435
21. Sheldrick GM (2008) *Acta Cryst A* 64:112–122
22. Farrugia LJ (1999) *J Appl Cryst* 32:837–838
23. Fulmer GR, Miller AJM, Sherden NH, Gottlieb HE, Nudelman A, Stoltz BM, Bercaw JE, Goldberg KI (2010) *Organometallics* 29:2176–2179
24. Atkins P, De Paula J (2006) *Physical chemistry*, 8th edn. W. H. Freeman, New York
25. Bain AD (2003) *Prog Nucl Magn Reson Spectrosc* 43:63–103
26. Sandström J (1982) *Dynamic NMR spectroscopy*. Academic Press, London
27. Hiraoka S, Okuno E, Tanaka T, Shiro M, Shionoya M (2008) *J Am Chem Soc* 130:9089–9098
28. Hiraoka S, Hisanaga Y, Shiro M, Shionoya M (2010) *Angew Chem Int Ed* 49:1669–1673
29. Kilbas B, Mirtschin S, Scopellitia R, Severin K (2012) *Chem Sci* 3:701–704
30. Leigh DA, Morales MAF, Pérez EM, Wong JKY, Saiz CG, Slawin AMZ, Carmichael AJ, Haddleton DM, Brouwer AM, Buma WJ, Wurpel GWH, León S, Zerbetto F (2005) *Angew Chem Int Ed* 44:3062–3067
31. Gong C, Gibson HW (1997) *Angew Chem Int Ed Engl* 36:2331–2333
32. Wilmes GM, France MB, Lynch SR, Waymouth RM (2004) *Organometallics* 23:2405–2411
33. Tafazzoli M, Ziyaei-Halimjani A, Ghiasi M, Fattahi M, Saidi MR (2008) *J Mol Struct* 886:24–31
34. Gennari M, Lanfranchi M, Cammi R, Pellinghelli MA, Marchiò L (2007) *Inorg Chem* 46:10143–10152
35. Nakafuji S, Kobayashi J, Kawashima T, Schmidt MW (2005) *Inorg Chem* 44:6500–6502
36. Blom R, Swang O (2002) *Eur J Inorg Chem* 411–415
37. Nomoto K, Kume S, Nishihara H (2009) *J Am Chem Soc* 131:3830–3831
38. Kume S, Nomoto K, Kusamoto T, Nishihara H (2009) *J Am Chem Soc* 131:14198–14199
39. Kume S, Nishihara H (2011) *Chem Commun* 47:415–417
40. Kume S, Nishihara H (2011) *Dalton Trans* 40:2299–2305

Photofunctionalization of Molecular Switch Based on
Pyrimidine Ring Rotation in Copper Complexes

Nishikawa, M.

2014, XII, 123 p. 105 illus., 23 illus. in color., Hardcover

ISBN: 978-4-431-54624-5